Nuclear Data for the Next Decade

Spin and Deformation of Fission Fragments

Guillaume SCAMPS

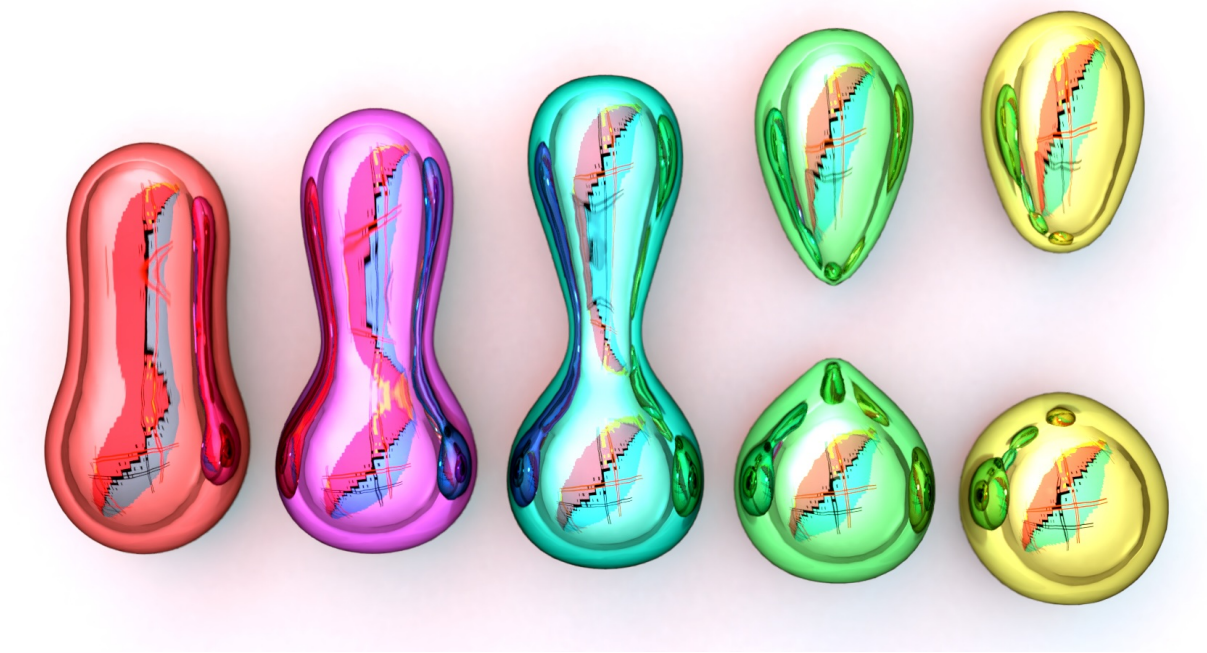

Université de Toulouse

L2IT

cnrs

TDHFB equations

$$i\hbar\frac{\partial}{\partial t}\begin{pmatrix} U \\ V \end{pmatrix} = \begin{pmatrix} h(t) & \Delta(t) \\ -\Delta^*(t) & -h^*(t) \end{pmatrix}\begin{pmatrix} U \\ V \end{pmatrix}$$

TDHFB equations

$$i\hbar\frac{\partial}{\partial t}\begin{pmatrix} U \\ V \end{pmatrix} = \begin{pmatrix} h(t) & \Delta(t) \\ -\Delta^*(t) & -h^*(t) \end{pmatrix}\begin{pmatrix} U \\ V \end{pmatrix}$$

Strengths

- Self-consistent mean field + pairing
- Functional and no other adjustable parameters.
- One-body dissipation
- Large-amplitude collective motion

TDHFB equations

$$i\hbar\frac{\partial}{\partial t}\begin{pmatrix} U \\ V \end{pmatrix} = \begin{pmatrix} h(t) & \Delta(t) \\ -\Delta^*(t) & -h^*(t) \end{pmatrix}\begin{pmatrix} U \\ V \end{pmatrix}$$

Strengths

- Self-consistent mean field + pairing
- Functional and no other adjustable parameters.
- One-body dissipation
- Large-amplitude collective motion

Weaknesses

- Missing quantum and statistic fluctuations
- Broken symmetries (projection needed)
- Computationally expensive

TDHFB equations

$$i\hbar\frac{\partial}{\partial t}\begin{pmatrix} U \\ V \end{pmatrix} = \begin{pmatrix} h(t) & \Delta(t) \\ -\Delta^*(t) & -h^*(t) \end{pmatrix}\begin{pmatrix} U \\ V \end{pmatrix}$$

TDBCS approximation

Canonical basis evolution :

$$i\hbar\,\dot{\varphi}_\alpha = h\,\varphi_\alpha$$

$$i\hbar\,\dot{n}_\alpha = \kappa_\alpha\Delta^*_\alpha - \kappa^*_\alpha\Delta_\alpha$$

$$i\hbar\,\dot{\kappa}_\alpha = 2\epsilon_\alpha\kappa_\alpha + \Delta_\alpha(2n_\alpha - 1)$$

Strengths

- Self-consistent mean field + pairing
- Functional and no other adjustable parameters.
- One-body dissipation
- Large-amplitude collective motion

Weaknesses

- Missing quantum and statistic fluctuations
- Broken symmetries (projection needed)
- Computationally expensive

First : CHF+BCS

Example : ^{240}Pu

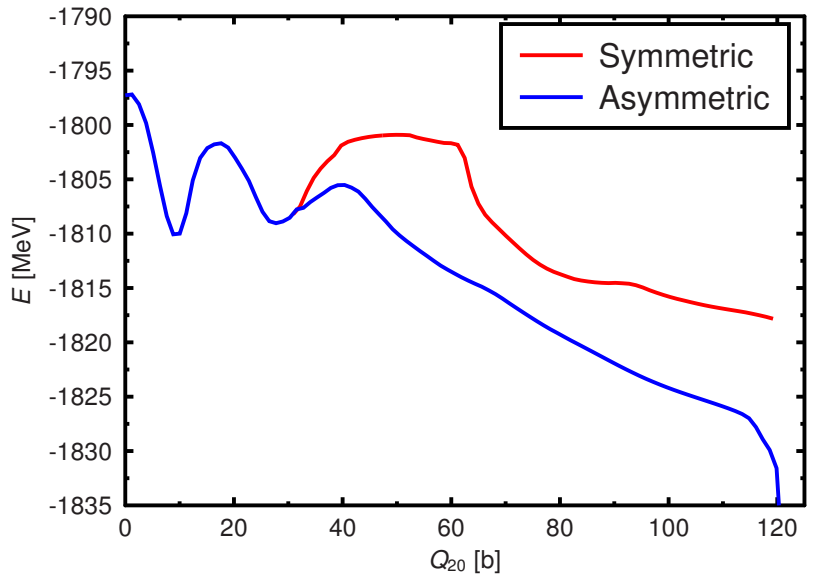

Second : TDHF+BCS

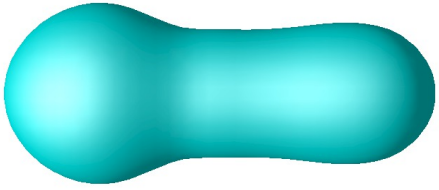

First : CHF+BCS

Example : ^{240}Pu

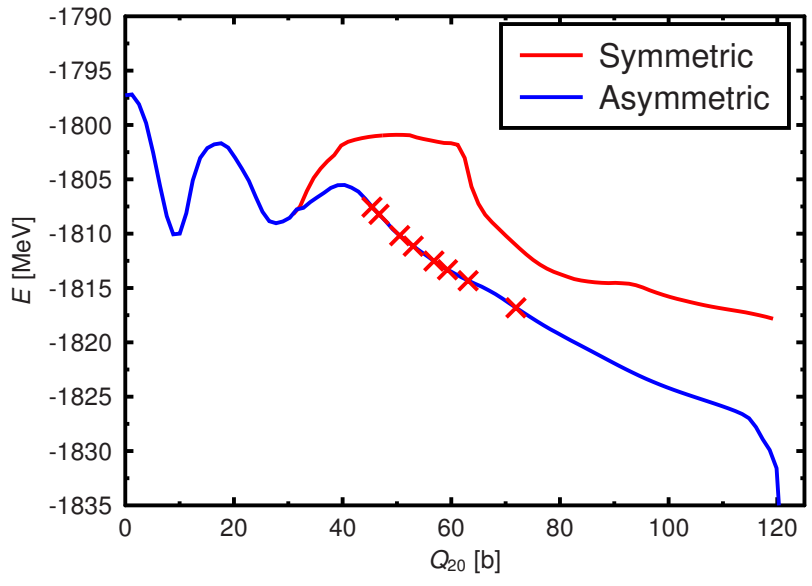

Second : TDHF+BCS

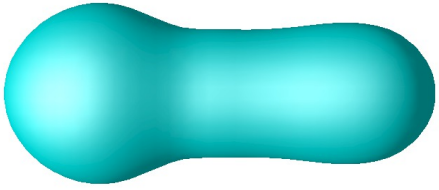

First : CHF+BCS

Example : ^{240}Pu

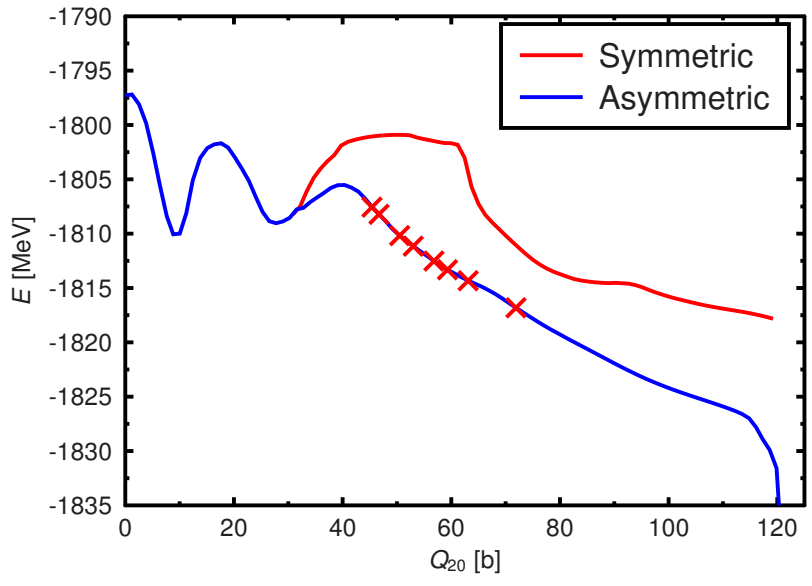

Second : TDHF+BCS

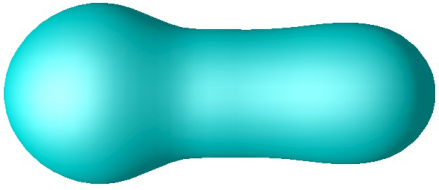

TDHF+BCS

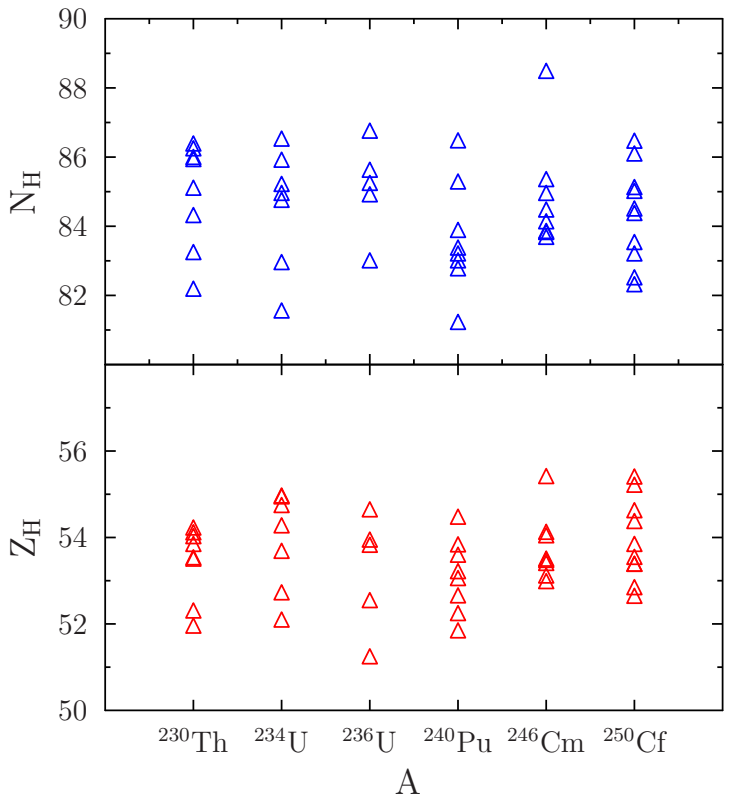

Comparison with experimental data

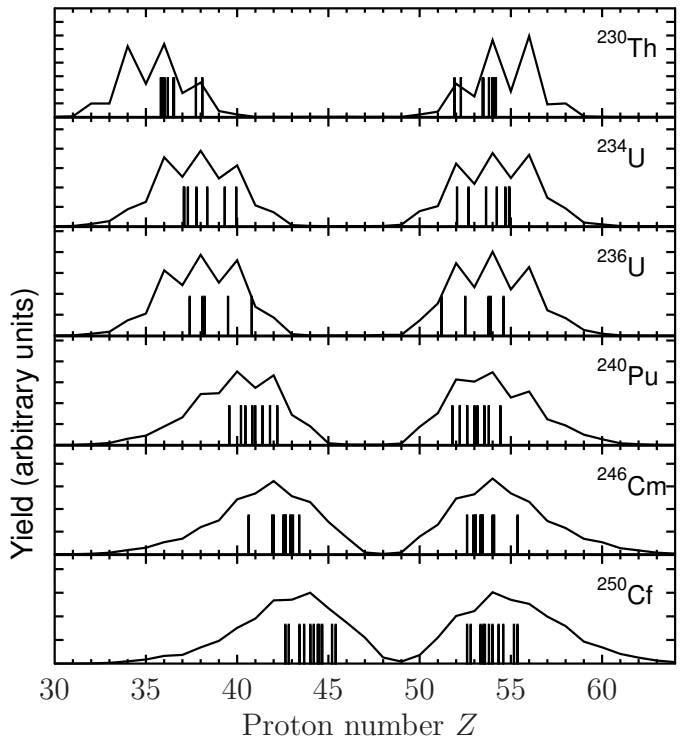

TDHF+BCS

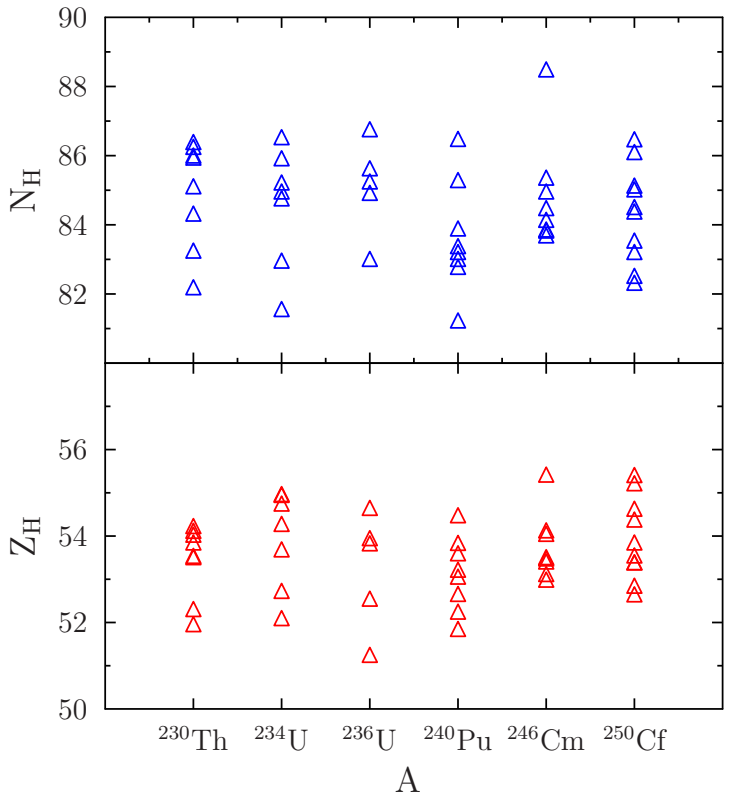

Comparison with experimental data

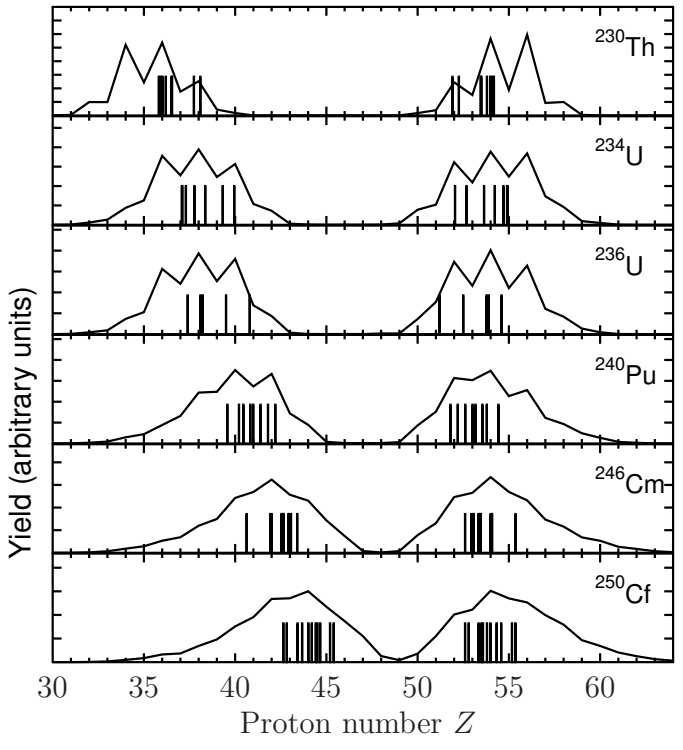

Conclusion :

The TDHF+BCS calculation reproduces well the Z=54 behavior. But why ?

^{240}Pu

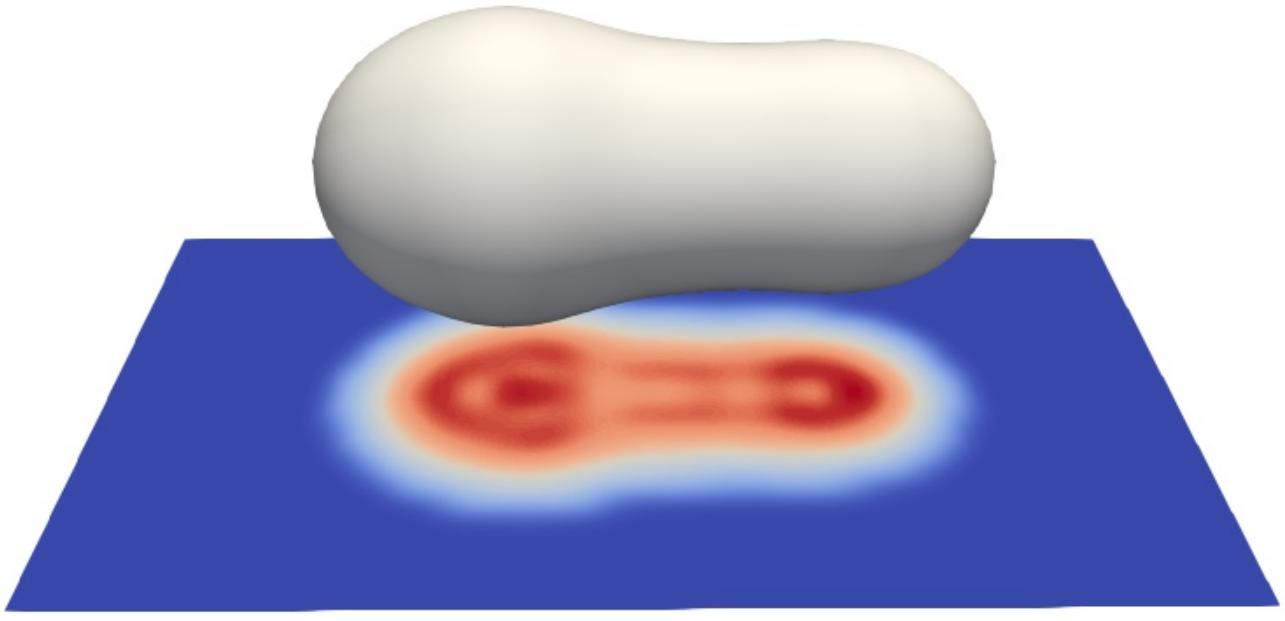

^{240}Pu

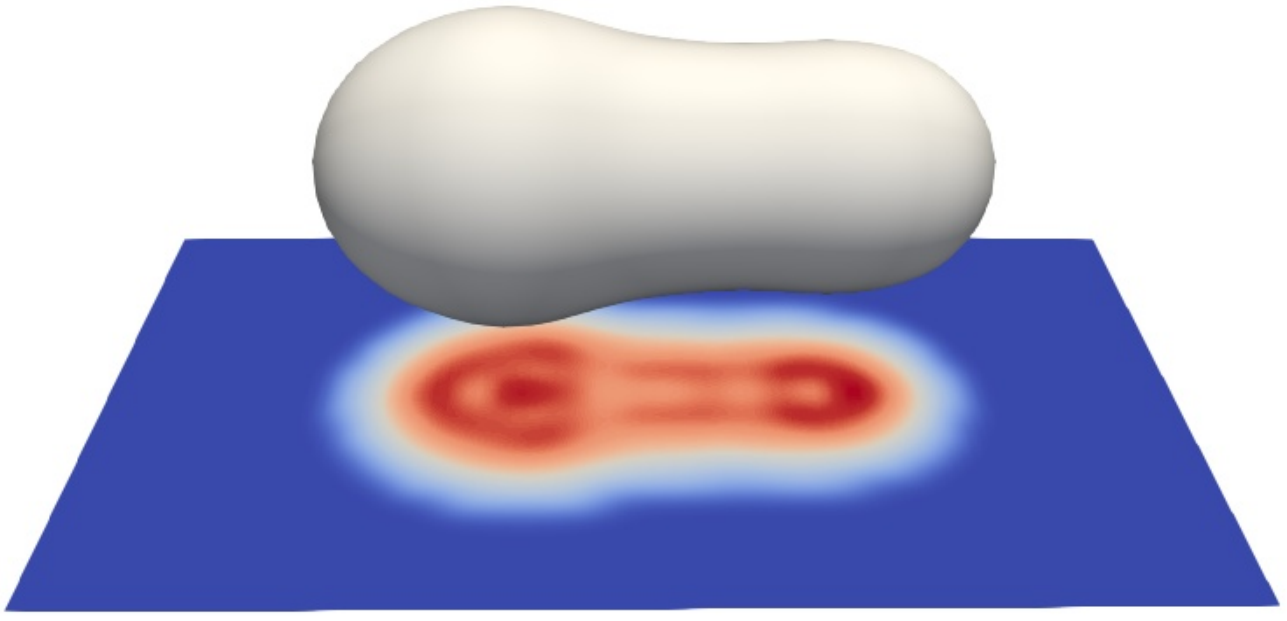

^{240}Pu

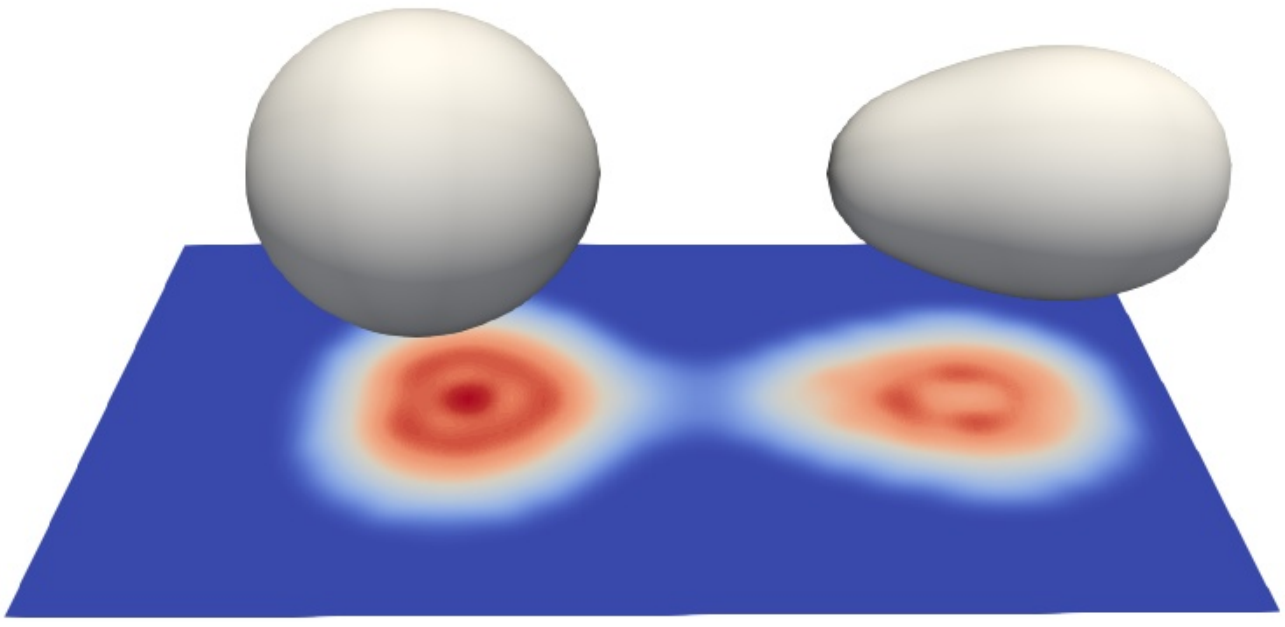

^{240}Pu

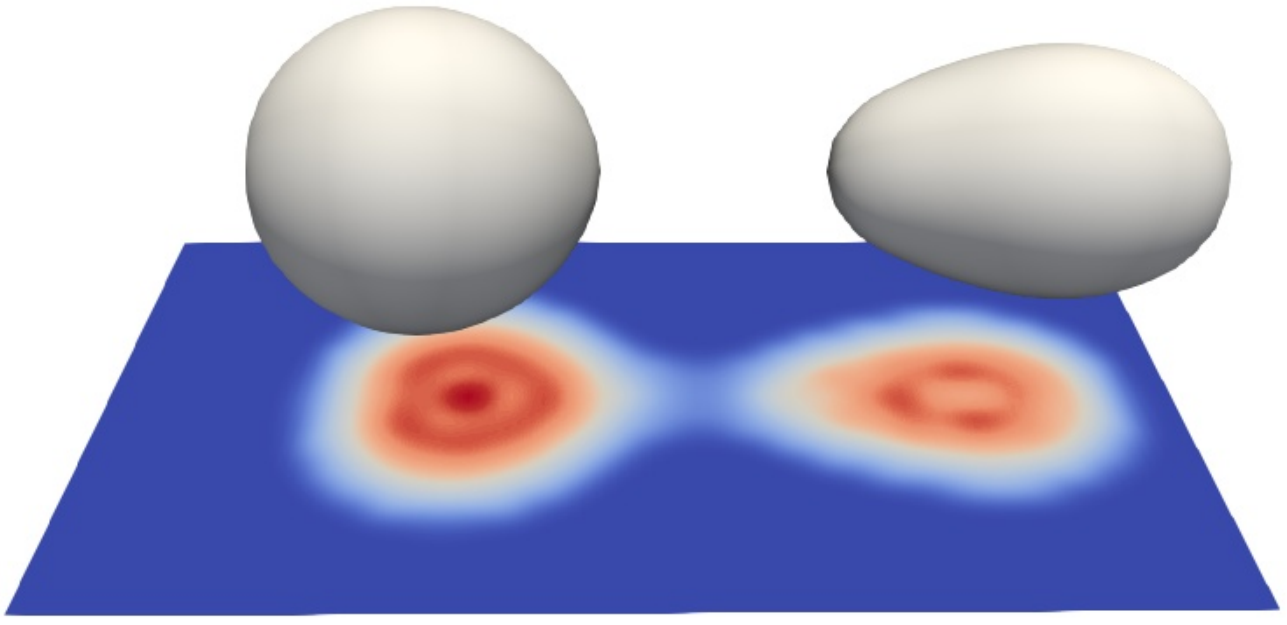

Other systems

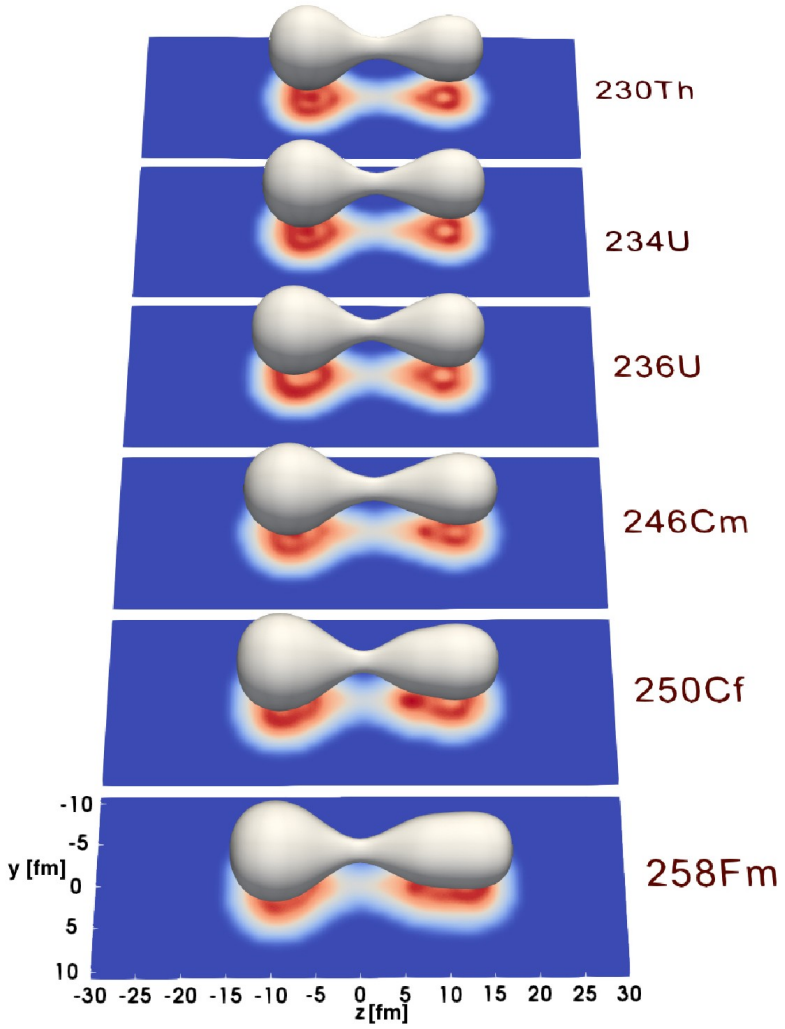

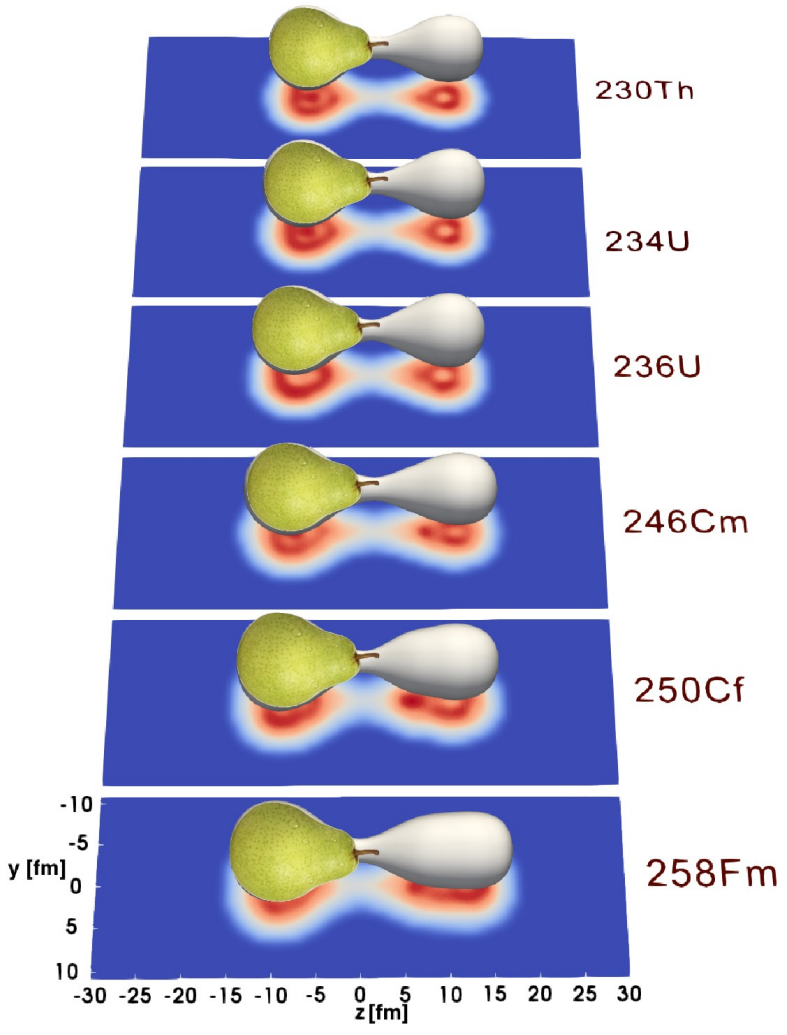
230Th
234U
236U
246Cm
250Cf
258Fm
y [fm]
-10
-5
0
5
10
-30 -25 -20 -15 -10 -5 0 5 10 15 20 25 30
z [fm]

Similar effect on fusion reaction :

^{40}Ca+^{40}Ca, $E3^-$ = 3.7 MeV

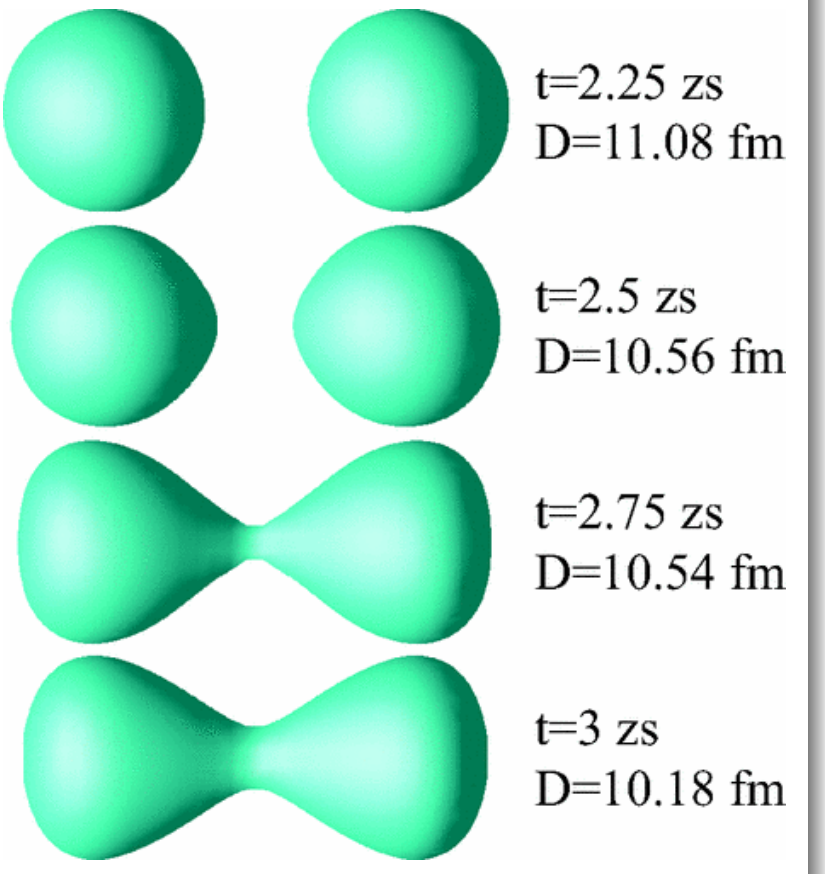

^{56}Ni+^{56}Ni, $E3^-$ = 7.5 MeV

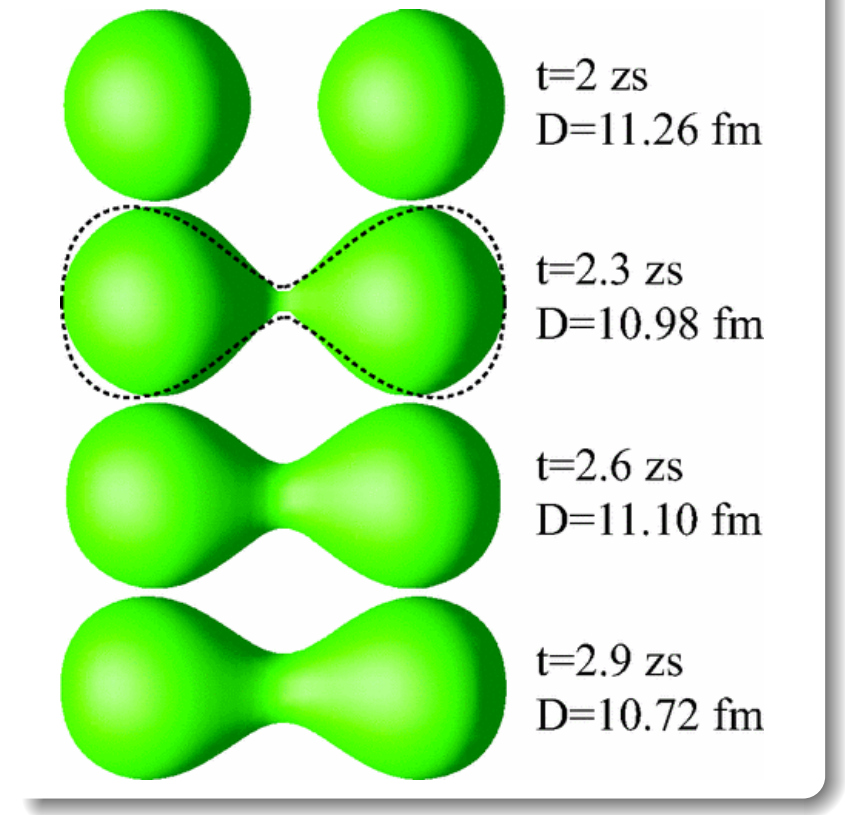

C. Simenel, M. Dasgupta, D. J. Hinde, and E. Williams, Phys. Rev. C 88, 064604 (2013).

Similar effect on fusion reaction :

^{40}Ca+^{40}Ca, $E3^-$ = 3.7 MeV

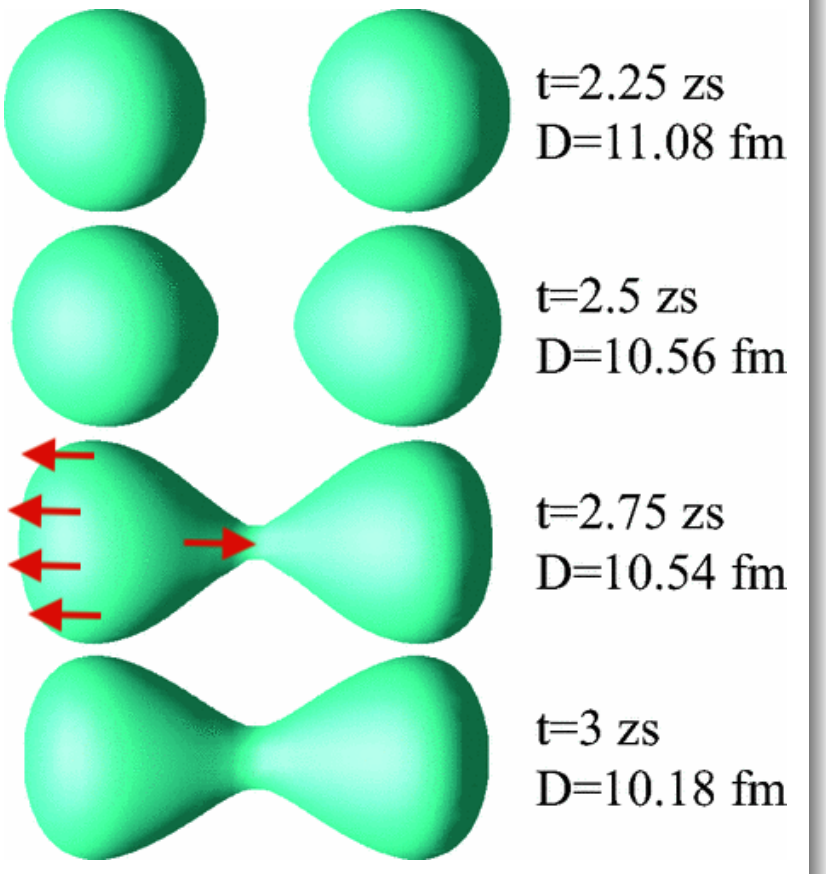

^{56}Ni+^{56}Ni, $E3^-$ = 7.5 MeV

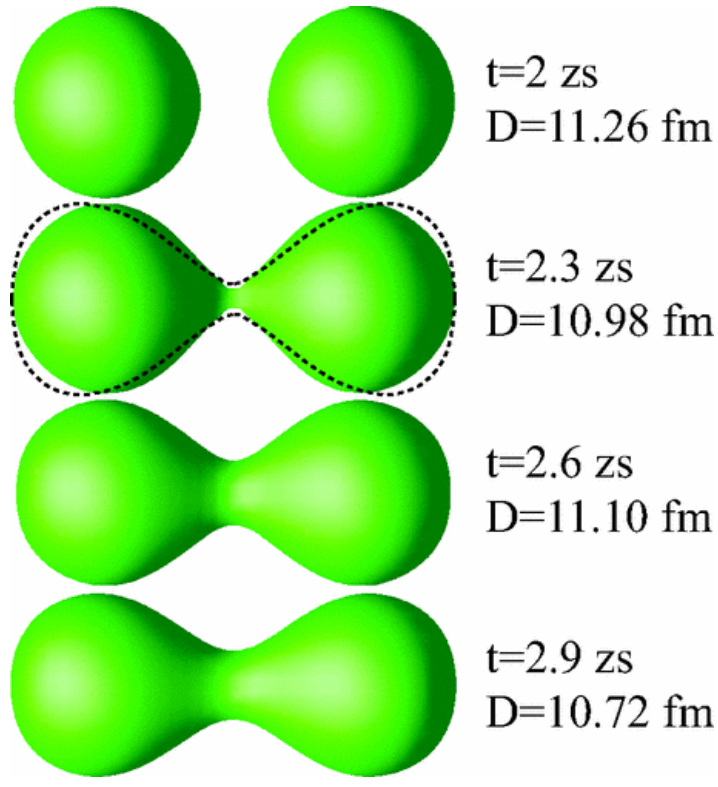

C. Simenel, M. Dasgupta, D. J. Hinde, and E. Williams, Phys. Rev. C 88, 064604 (2013).

Skyrme Skm*.

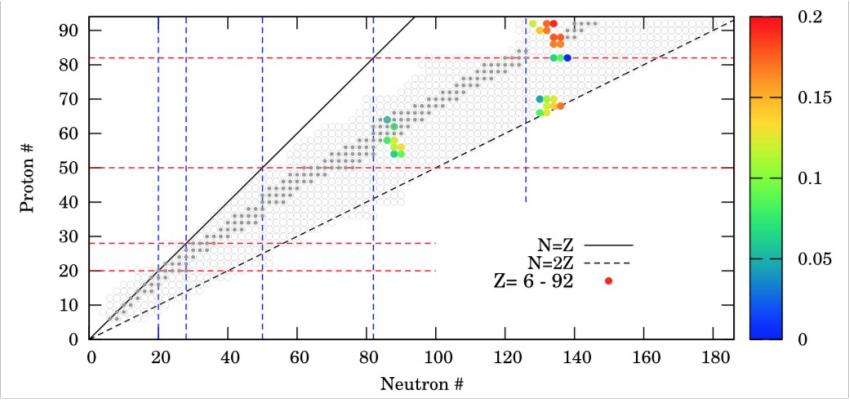

S. Ebata, and T. Nakatsukasa, Phys. Scr. 92 (2017)

Gogny D1S

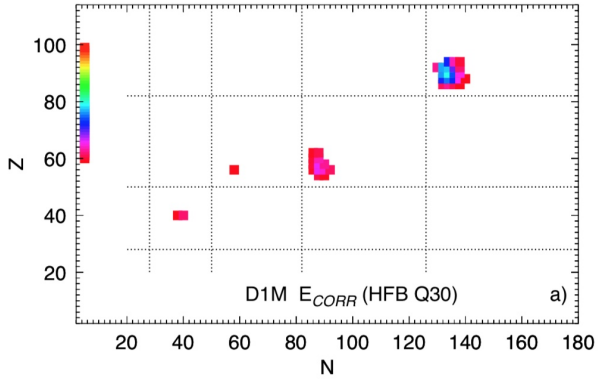

LM Robledo - J. phys. G : Nucl. and Part. Phys. (2015)

Results from systematic calculation

In both calculations, the region Z $\simeq$ 56, N $\simeq$ 88 is favorable for octupole deformation.

Experimental results

^{144}Ba is found to be octupole in its ground state. Burcher et al. PRL 116 (2016).

Skyrme Skm*.

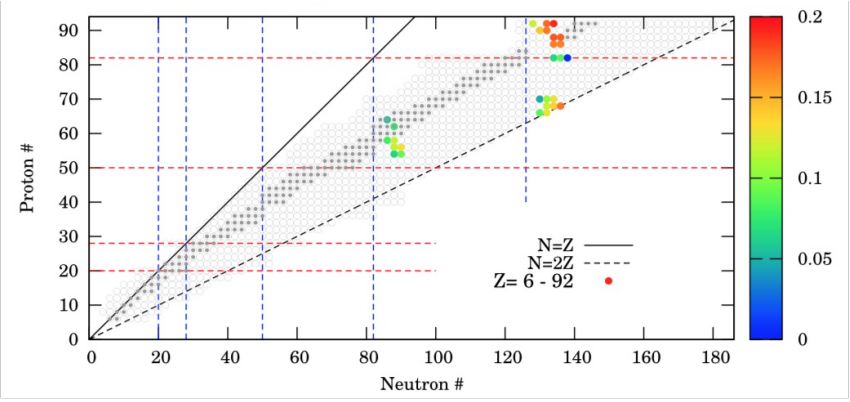

S. Ebata, and T. Nakatsukasa, Phys. Scr. 92 (2017)

Fission data

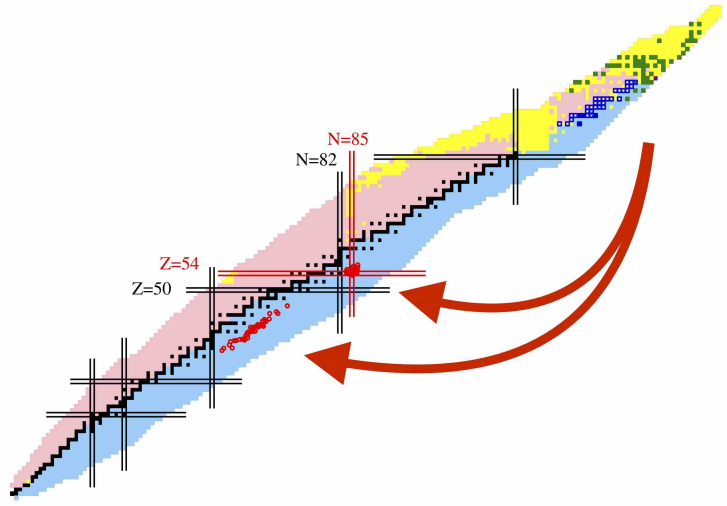

Results from systematic calculation

In both calculations, the region $Z \simeq 56$, $N \simeq 88$ is favorable for octupole deformation.

Experimental results

^{144}Ba is found to be octupole in its ground state. Burcher et al. PRL 116 (2016).

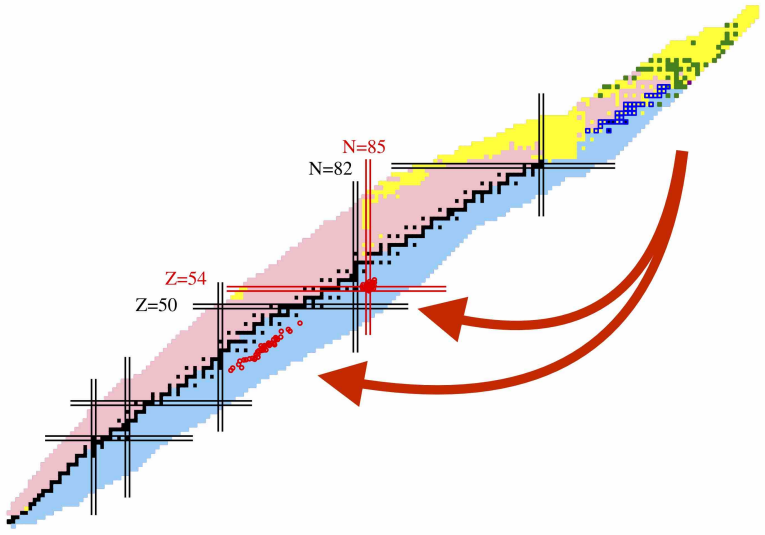

Mechanism

- The Nucleus-Nucleus interaction at the scission configuration favors the octupole shapes
- Shell structure favors octupole shape in the region Z $\simeq$ 52-56, N $\simeq$ 84-88
- Actinide fission fragments are driven in the region Z $\simeq$ 54, N $\simeq$ 86

G. Scamps, C. Simenel, Nature 564, 382 (2018).

Spin of the fragments

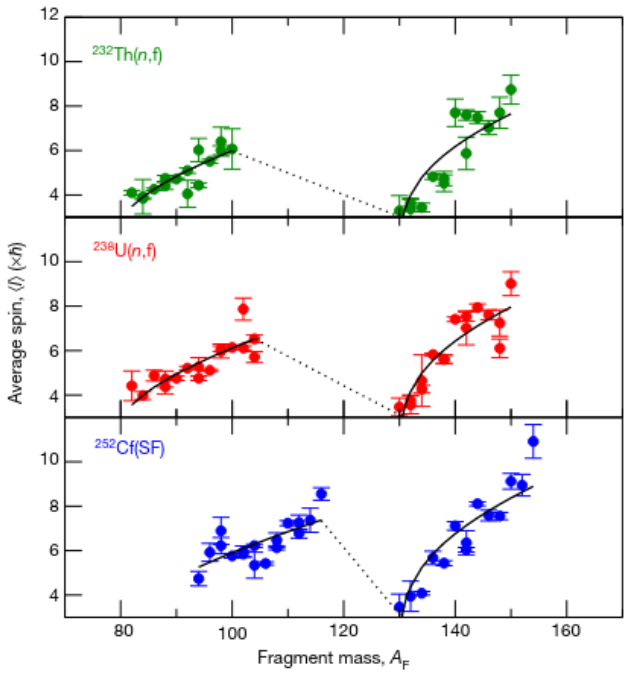

Correlations

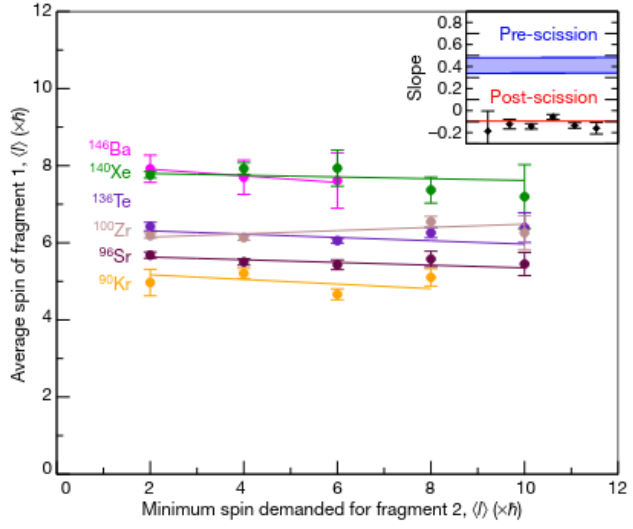

J. N. Wilson, Nature, 590, 566 (2021)

- The average spin follows a sawtooth shape
- No correlations between the spins of the fragments

Literature

- Thermal excitations
- Quantum fluctuations
- Coulomb force
- Breaking of the neck

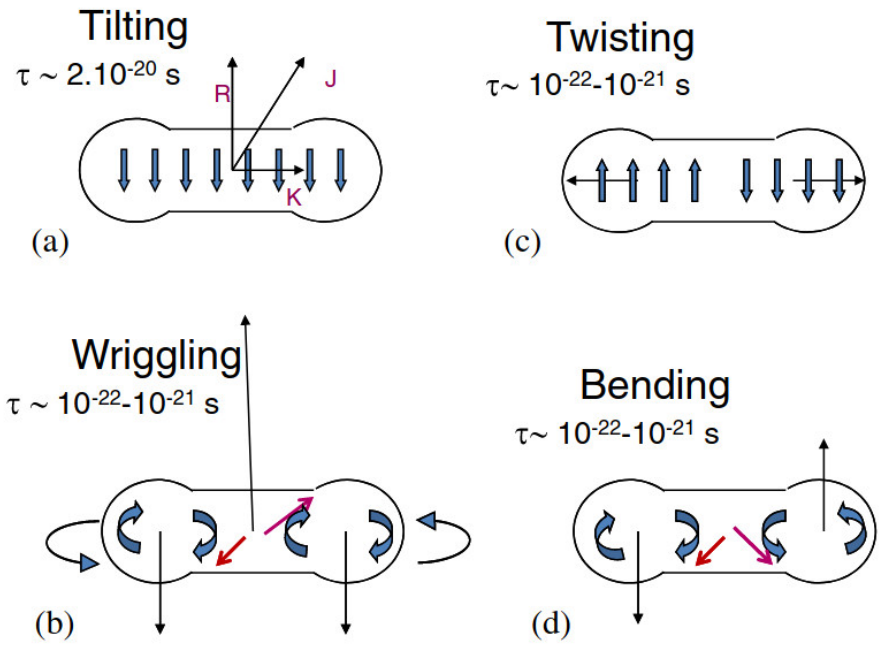

Illustration from B. John, J. Phys., 85, 2, (2015).

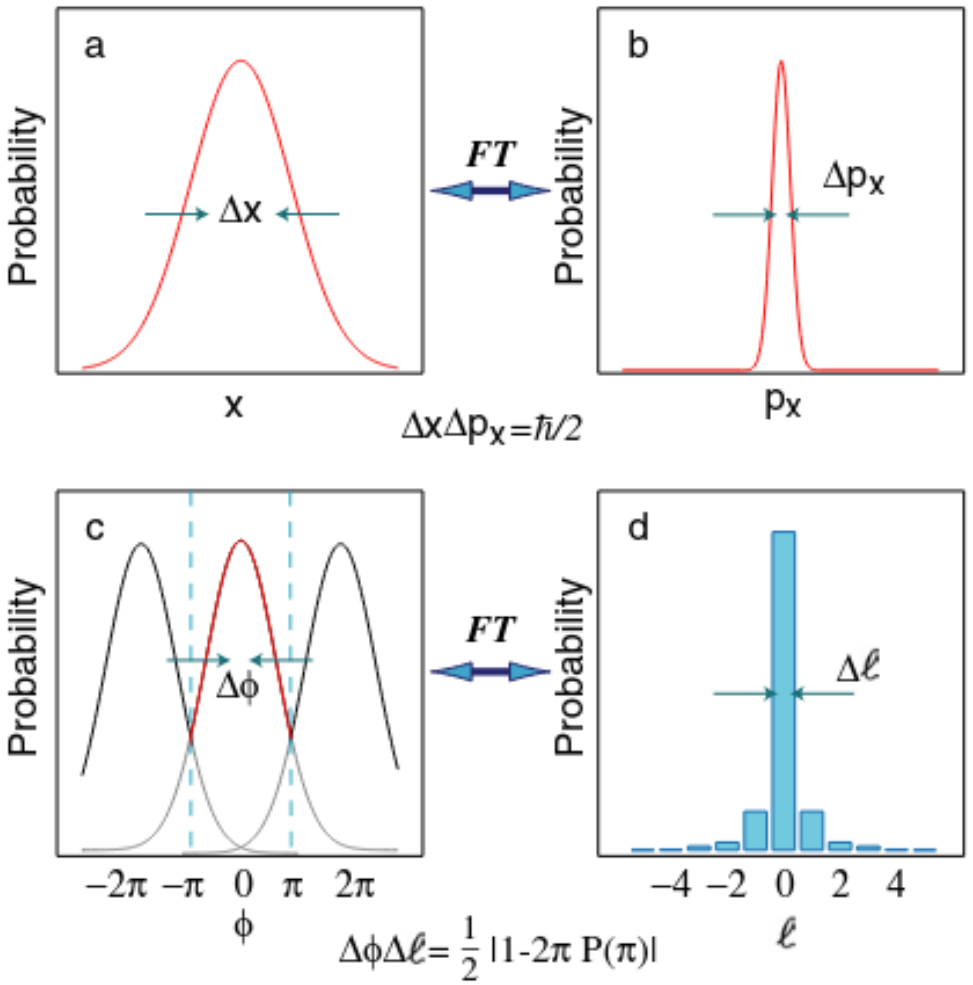

S. Franke-Arnold, et al. New Journal of Physics 6, 103 (2004)

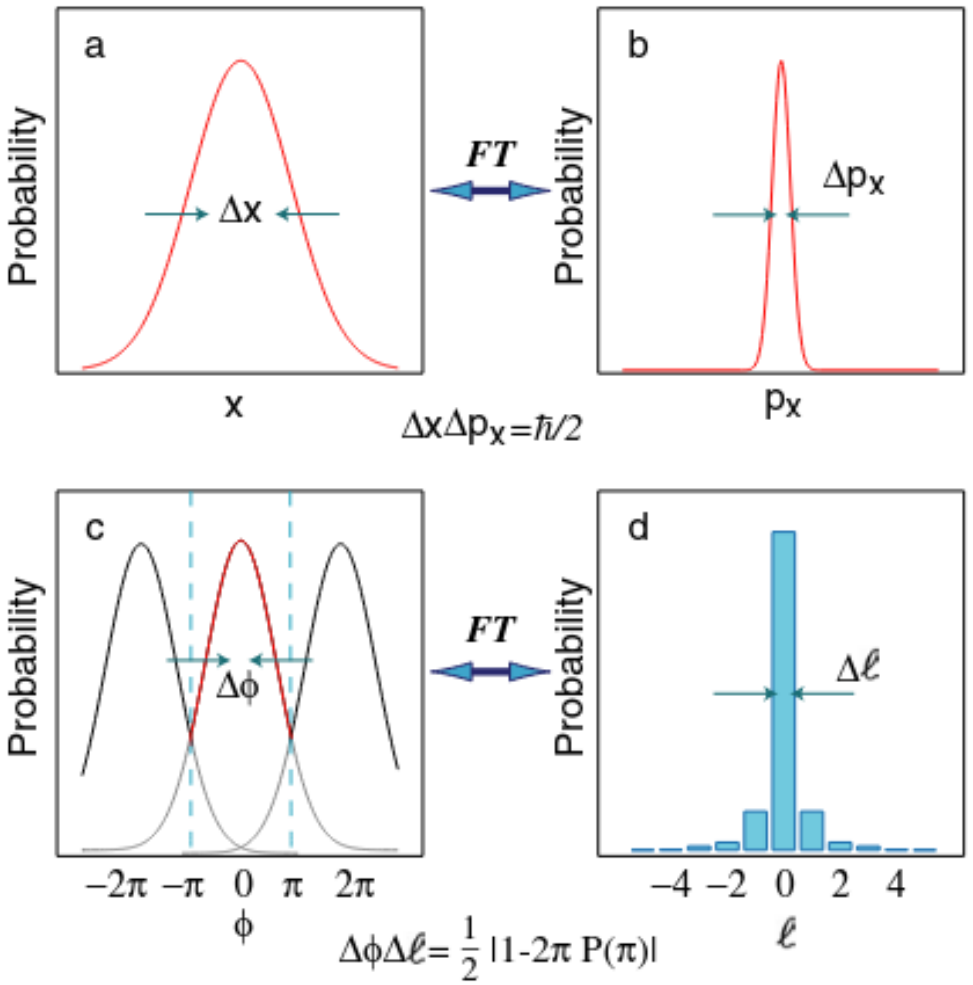

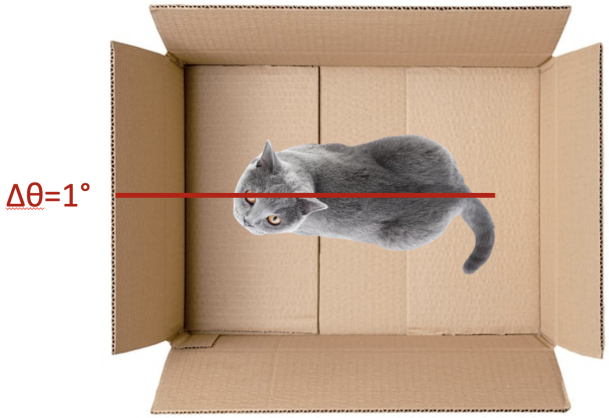

S. Franke-Arnold, et al. New Journal of Physics 6, 103 (2004)

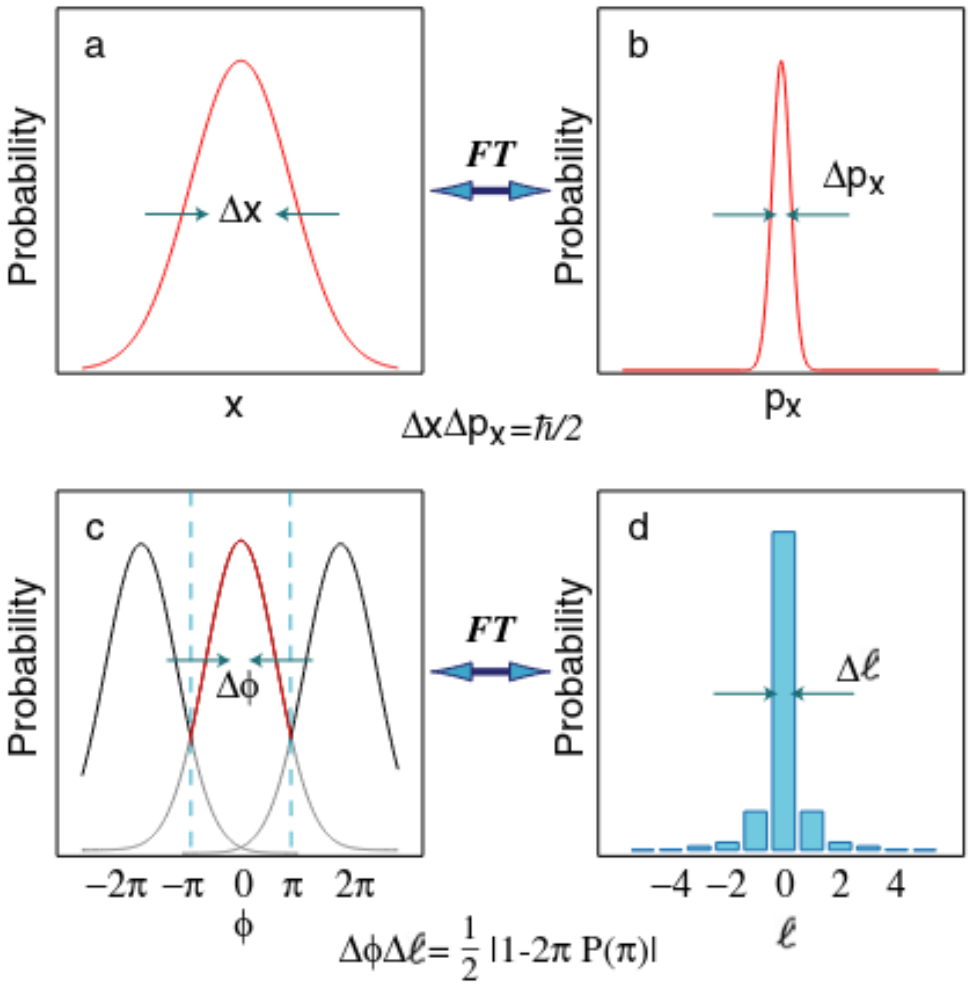

S. Franke-Arnold, et al. New Journal of Physics 6, 103 (2004)

For $\Delta\Theta = 1^\circ$, $\Delta L = 29\hbar$.
For a cat, angular velocity $\omega = 10^{-33} s^{-1}$

Premiers harmoniques sphériques

	$m=-3$	$m=-2$	$m=-1$	$m=0$	$m=+1$	$m=+2$	$m=+3$
$\ell=0$				$\frac{1}{\sqrt{4\pi}}$			
$\ell=1$			$\frac{1}{\sqrt{4\pi}}\sqrt{\frac{3}{2}}\sin\theta e^{-i\phi}$	$\frac{1}{\sqrt{4\pi}}\sqrt{3}\cos\theta$	$\frac{1}{\sqrt{4\pi}}\sqrt{\frac{3}{2}}\sin\theta e^{i\phi}$		
$\ell=2$		$\frac{1}{\sqrt{4\pi}}\frac{\sqrt{15}}{2^{3/2}}\sin^2\theta e^{-i2\phi}$	$\frac{1}{\sqrt{4\pi}}\frac{\sqrt{15}}{2}\cos\theta\sin\theta e^{-i\phi}$	$\frac{1}{\sqrt{4\pi}}\frac{\sqrt{5}}{2}\left(3\cos^2\theta-1\right)$	$\frac{1}{\sqrt{4\pi}}\frac{\sqrt{15}}{2}\cos\theta\sin\theta e^{+i\phi}$	$\frac{1}{\sqrt{4\pi}}\frac{\sqrt{15}}{2^{3/2}}\sin^2\theta e^{+i2\phi}$	
$\ell=3$							

Orientation pumping mechanism

Isotropic potential at scission

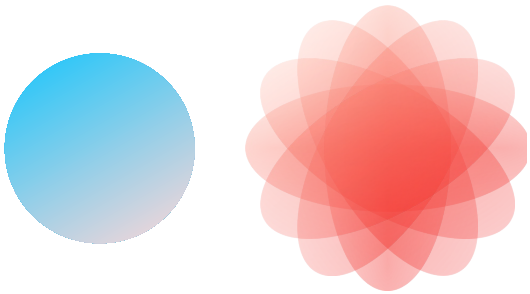

Confining potential at scission

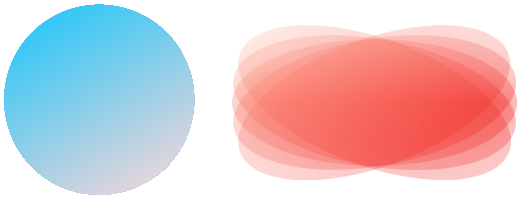

L. Bonneau, P. Quentin, and I. N. Mikhailov, PRC 75, 064313 (2007).

For $\Delta\Theta = 1^\circ$, $\Delta L = 29\hbar$.

For a nucleus, angular velocity $\omega = 10^{20} s^{-1}$

Static HFB

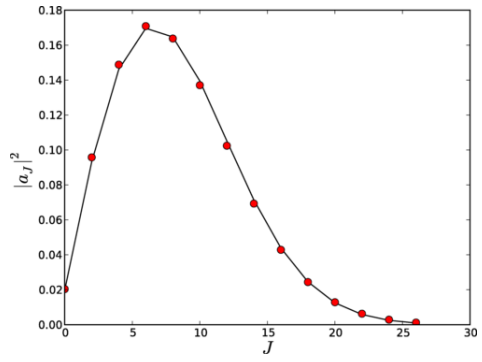

G. F. Bertsch, T. Kawano, and L. M. Robledo, PRC 99, 034603 (2019)

TDHFB - TDSLDA

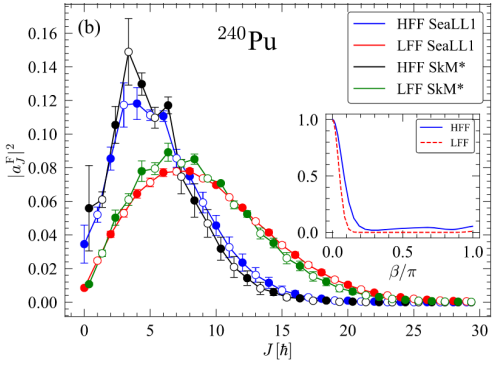

A. Bulgac, et al., PRL 126, 142502 (2021)

Scission configuration

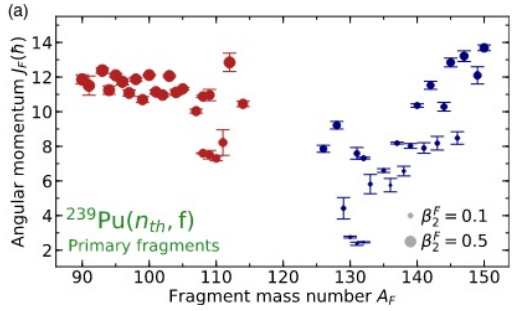

P. Marević, N. Schunck, J. Randrup, and R. Vogt PRC 104, L021601 (2021).

Projection method

$$\hat{P}_J\left(|\Psi(J=0)\rangle + |\Psi(J=1)\rangle + \ldots\right) = |\Psi(J)\rangle$$

$$|a_J^F|^2 = \frac{2J+1}{2}\int_0^{2\pi} \sin(\beta)\, P_J(\cos(\beta))\langle\Psi|e^{\frac{-i\hat{J}_x^F\beta}{\hbar}}|\Psi\rangle$$

Conceptual difficulty

- Unlike position, angular variables are **periodic**.
- Mean values and fluctuations of an angle are not uniquely defined.
- Restrict to well-oriented wave packet

Orientation–angular momentum uncertainty

$$\Delta\theta\,\Delta L_x > \frac{1}{2}, \qquad (L_x \text{ in units of } \hbar)$$

Analogous relation for L_y.

Gaussian orientation state and spin distribution

Gaussian wave packet :

$$\Psi(\theta,\varphi) = \mathcal{N}\exp\left[-\frac{\theta^2}{4\sigma_\theta^2}\right]$$

Spin cut-off distribution :

$$P(L) = \frac{2L+1}{\mathcal{Z}}\exp\left[-\frac{L(L+1)}{2\sigma_L^2}\right]$$

Heisenberg-type relation :

$$\sigma_\theta\,\sigma_L = \frac{1}{2}$$

Second difficulty : composite nuclei

- In collective Hamiltonian models, angle wave packets are well defined.
- In microscopic approaches, orientation is **not an operator**.
- Principal axis obtained from one-body density.
- No direct definition of angular fluctuations.

Proposed approach

- Go beyond the one-body density picture.
- Sample nucleon positions and intrinsic spins from the Bogoliubov vacuum.
- Markov Chain Monte Carlo sampling (`NucleoScope`).
- Determine principal axis event-by-event.

Principal axis determination

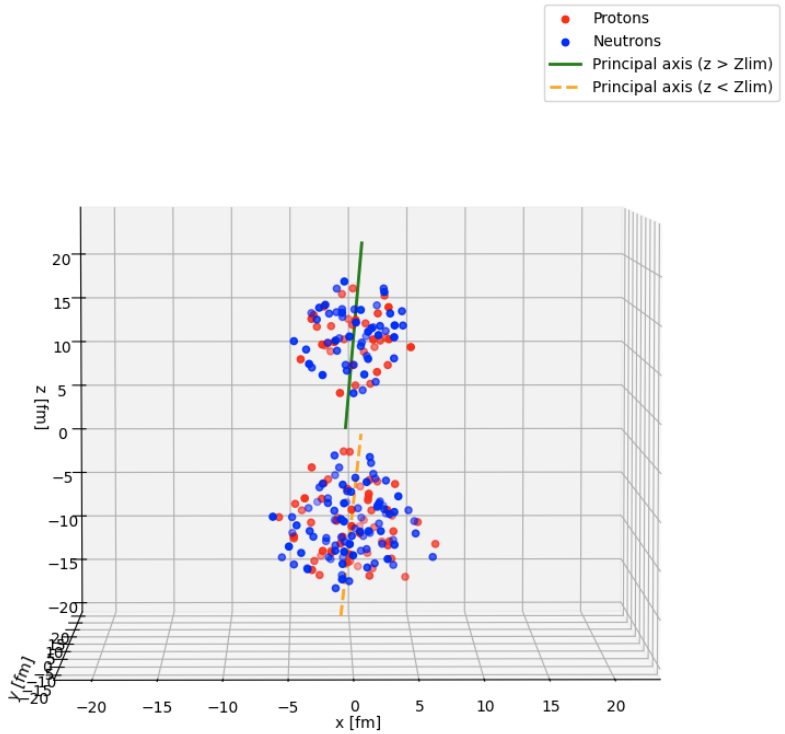

Examples for ^{230}Th.
Red/blue dots : proton/neutron distributions.
Lines : fragment principal axes.

Nucleoscope paper : A. Bernard *et al.*, arXiv :2601.18488 [nucl-th] (2026)

Second difficulty : composite nuclei

- In collective Hamiltonian models, angle wave packets are well defined.
- In microscopic approaches, orientation is **not an operator**.
- Principal axis obtained from one-body density.
- No direct definition of angular fluctuations.

Proposed approach

- Go beyond the one-body density picture.
- Sample nucleon positions and intrinsic spins from the Bogoliubov vacuum.
- Markov Chain Monte Carlo sampling (`NucleoScope`).
- Determine principal axis event-by-event.

Principal axis determination

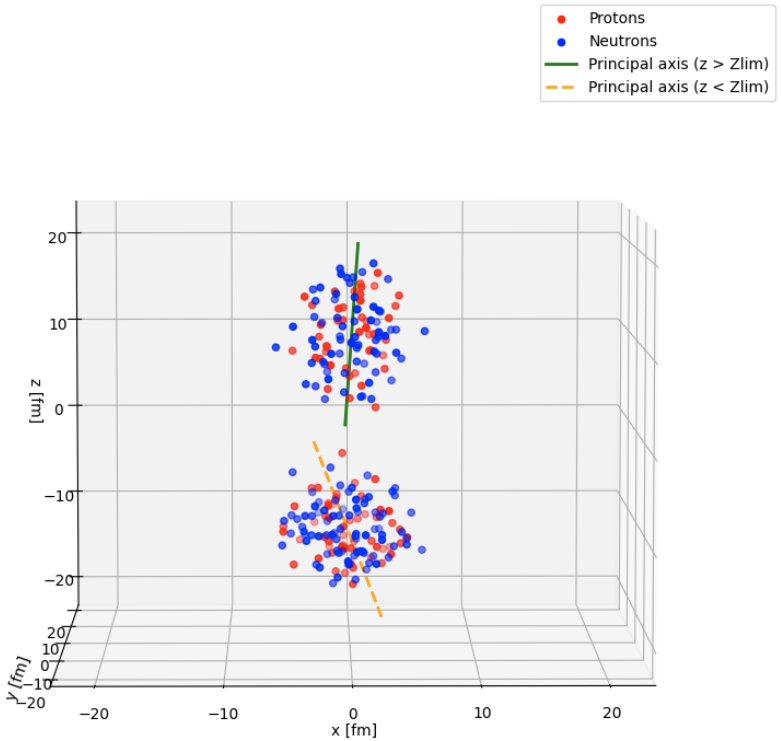

Examples for ^{230}Th.
Red/blue dots : proton/neutron distributions.
Lines : fragment principal axes.

Nucleoscope paper : A. Bernard *et al.*, arXiv :2601.18488 [nucl-th] (2026)

Distribution of θ

- For each sampled event, principal axis of each fragment is computed.
- Obtain θ = angle between fragment axis and global z-axis.
- Construct full probability distribution $P(\theta)$.
- Expectation value $\langle\theta\rangle = 0$ due to symmetry.
- Standard deviation σ_θ characterizes the angular fluctuation.

Physical meaning

- Reflects uncertainty in fragment orientation.
- Geometric definition mainly sensitive to quadrupole deformation.
- Can be used for spin-cutoff estimations.

Angular distribution figure

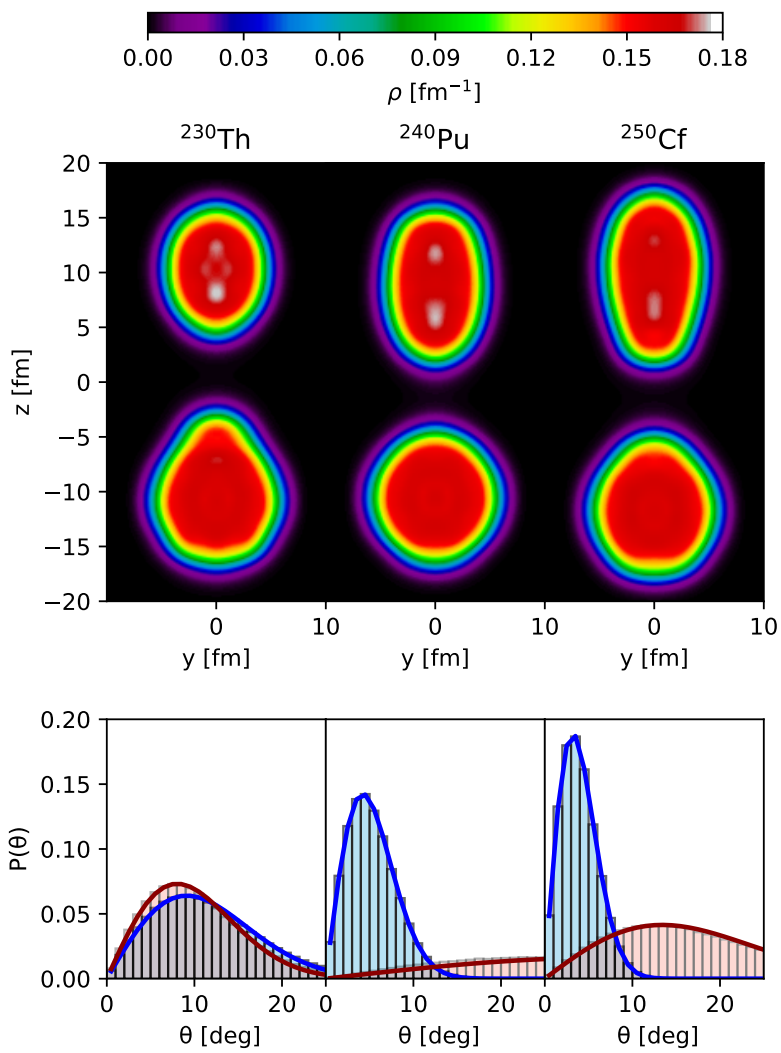

Angular distribution $P(\theta)$ for light (blue) and heavy (red) fragments. Fitted curves illustrate approximate Gaussian behavior.

Angular distribution

$$f(\theta) = \mathcal{N}^2 \sin(\theta) \exp\left[-\frac{\theta^2}{2\sigma_\theta^2}\right]$$

- Excellent agreement with Gaussian form
- Angular fluctuations are Gaussian
- Larger quadrupole deformation $\Rightarrow$ narrower distribution

From σ_θ to spin

$$\sigma_\theta \, \sigma_L = \frac{1}{2}$$

- Extract σ_θ
- Deduce spin cut-off σ_L
- Build spin distribution

Spin distribution

$$P(L) = \frac{2L+1}{\mathcal{Z}} \exp\left[-\frac{L(L+1)}{2\sigma_L^2}\right]$$

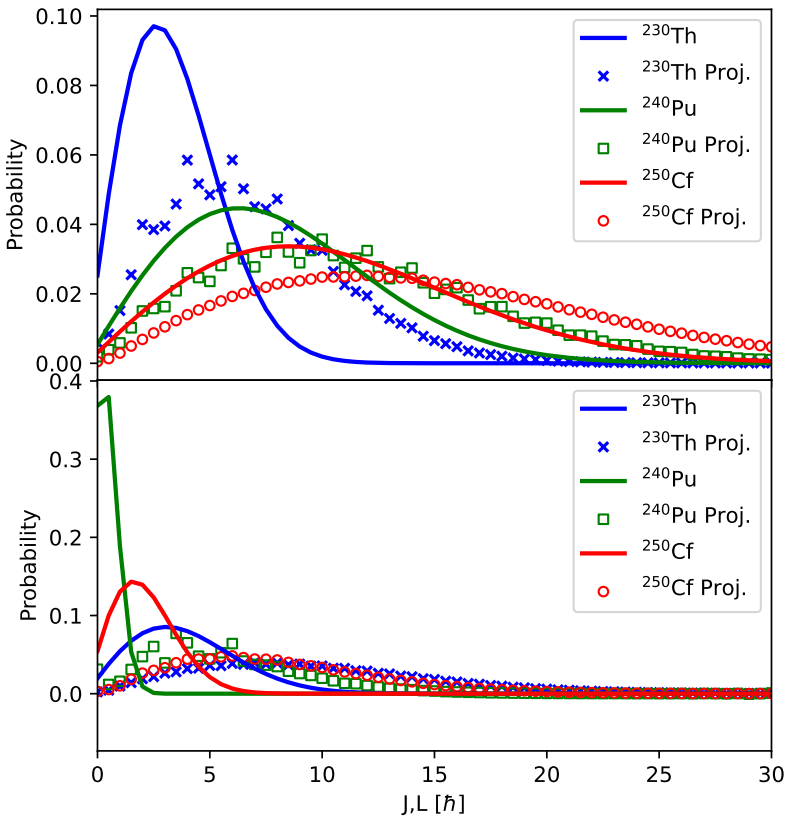

Projection results vs. spin cut-off formula (light : top, heavy : bottom).

Microscopic vs geometric picture

- Exact angular momentum obtained from projection of many-body states.
- Monte Carlo sampling determine the fluctuations of the fragment principal axis from Q_2 deformation.

Octupole deformation

- Principal axis distribution becomes flat.
- Geometric picture underestimates spin.

Spin-cutoff vs deformation

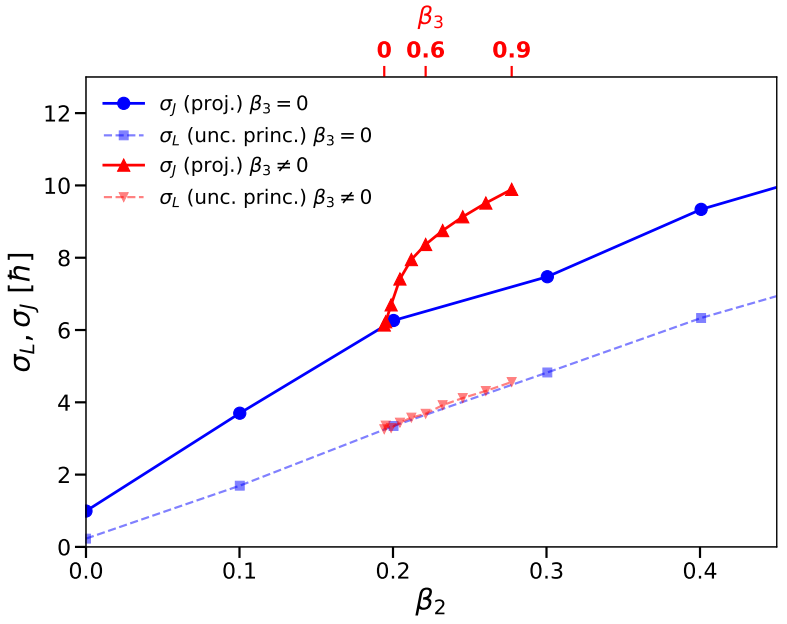

Spin cut-off parameter for ^{144}Ba. Solid lines : projection. Dashed lines : principal-axis uncertainty estimate.

Prolate deformation

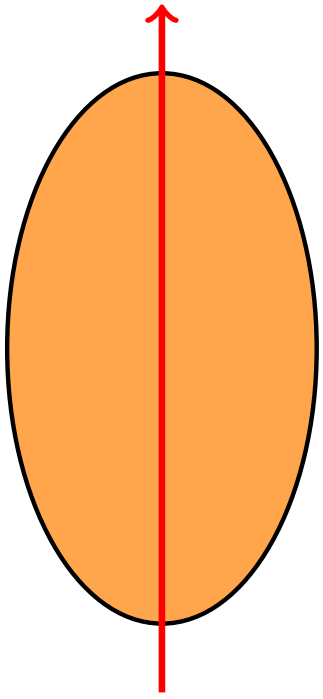

$Q_2 > 0$

Principal axis well defined

Triangular (octupole) configuration

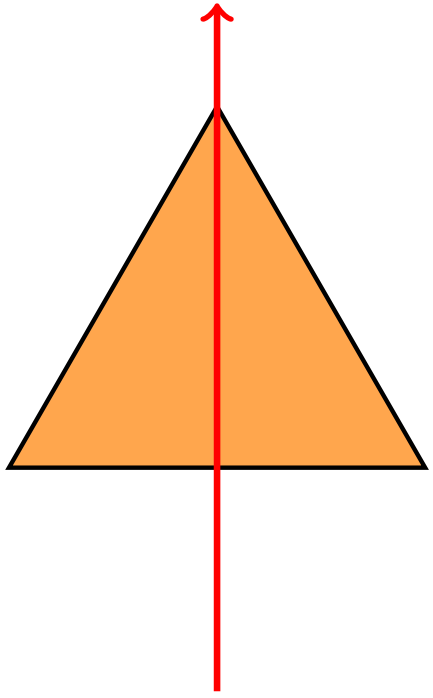

$Q_2 = 0$

Orientation still defined but principal axis isotropic

Overlap of rotated many-body states

$$\langle \Psi | e^{i\alpha \hat{J}_z} e^{i\theta \hat{J}_y} e^{i\gamma \hat{J}_z} | \Psi \rangle \simeq \exp\left[-\frac{\theta^2}{8\sigma_\theta^2} \right]$$

- Gaussian approximation for small rotations
- Width σ_θ characterizes angular localization

Physical meaning

- Many-body state localized in rotational space
- Does **not** rely on geometric definition of orientation
- Orientation angle and angular momentum are conjugate variables

Spin fluctuations

Spin cut-off distribution :

$$P(J) = \frac{2J+1}{\mathcal{Z}} \exp\left[-\frac{J(J+1)}{2\sigma_J^2} \right]$$

$$\sigma_\theta \, \sigma_J = \frac{1}{2}$$

Nucleus	Frag.	σ_L (uncert. with principal axis)	σ_J (overlap)	σ_J (projection)
^{230}Th	L	2.90	5.74	5.81
	H	3.37	7.84	7.88
^{240}Pu	L	6.79	9.32	9.37
	H	0.75	4.67	4.93
^{250}Cf	L	9.00	12.18	12.27
	H	2.12	6.50	6.63

Key result

- Spin cut-off parameters extracted from :
  - angular fluctuations + uncertainty relation
  - Gaussian overlap fit
  - exact angular-momentum projection
- **Excellent agreement** between overlap and exact projection.
- Error with the principal axis method (miss higher order deformation).

G. Scamps, A. Guilleux, D. Regnier, A. Bernard, Uncertainty Principle and Angular Momentum Generation in Microscopic Fission Models, arXiv :2512.02207 [nucl-th].

^{144}Ba + ^{96}Sr at 16 Fm, Θ_{ini}=25 deg, Functional : Skyrme Sly4d

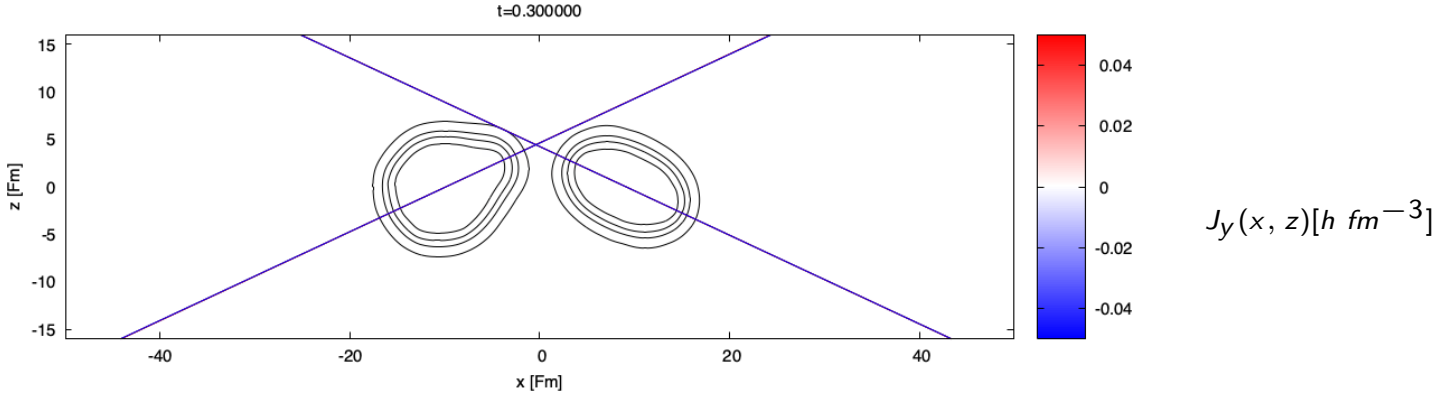

G. Scamps, PRC 106, 054614 (2022).

One body-evolution - One body-observable

^{144}Ba + ^{96}Sr at 16 Fm, Θ_{ini}=25 deg, Functional : Skyrme Sly4d

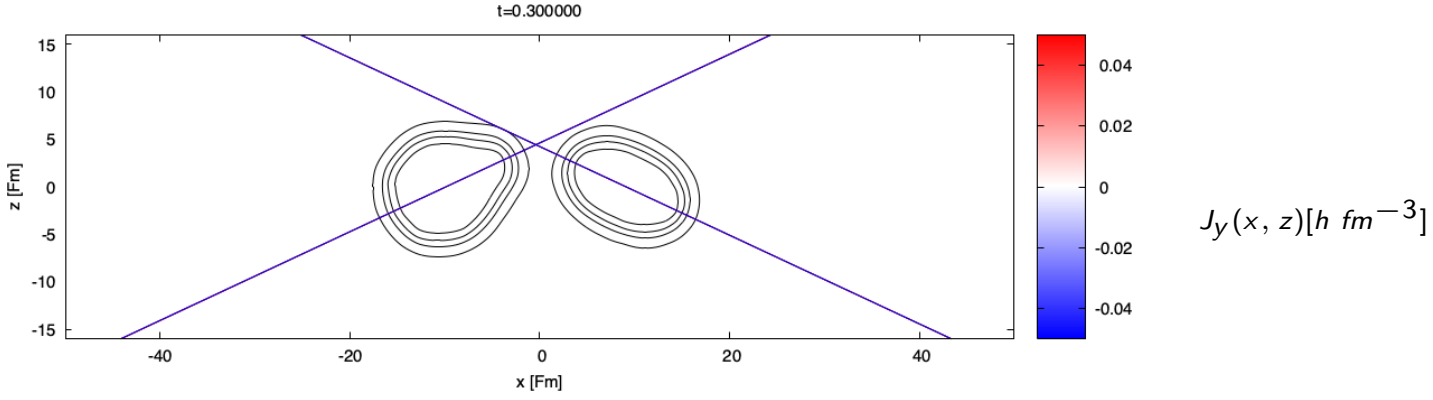

G. Scamps, PRC 106, 054614 (2022).

One body-evolution - One body-observable

^{144}Ba + ^{96}Sr at 16 Fm, Θ_{ini}=25 deg, Functional : Skyrme Sly4d

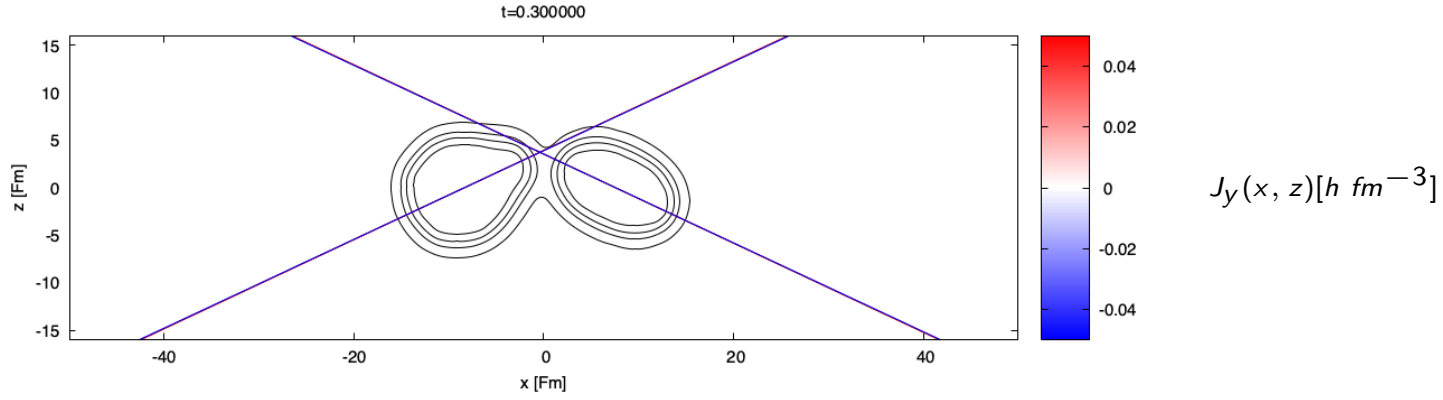

G. Scamps, PRC 106, 054614 (2022).

^{144}Ba + ^{96}Sr at 16 Fm, Θ_{ini}=25 deg, Functional : Skyrme Sly4d

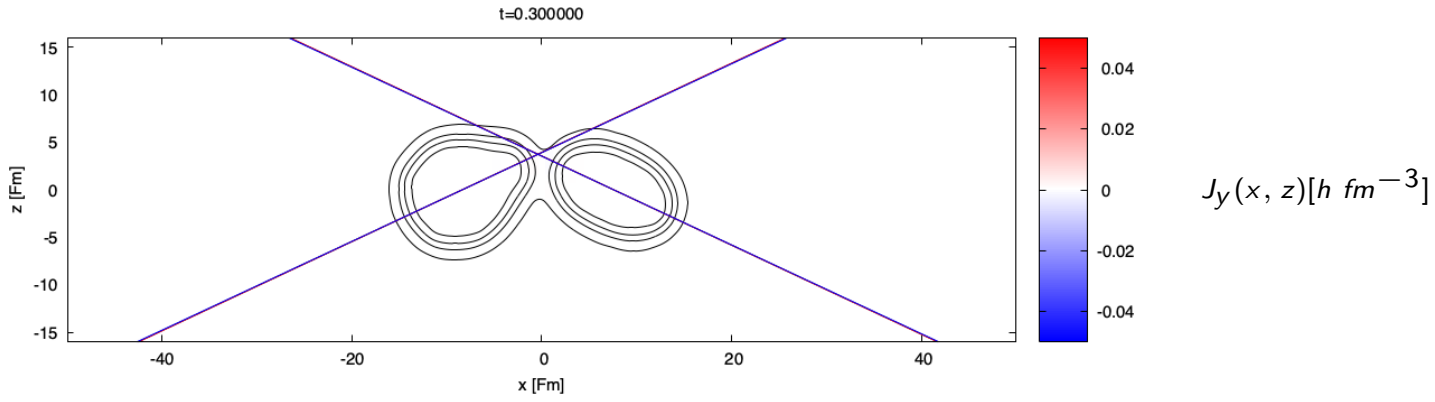

G. Scamps, PRC 106, 054614 (2022).

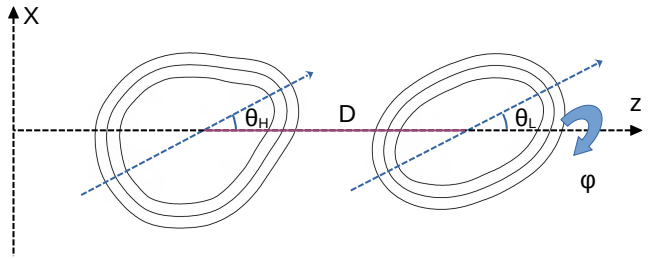

Potential as a function of the light fragment angle

$^{132}Sn + ^{108}Ru$

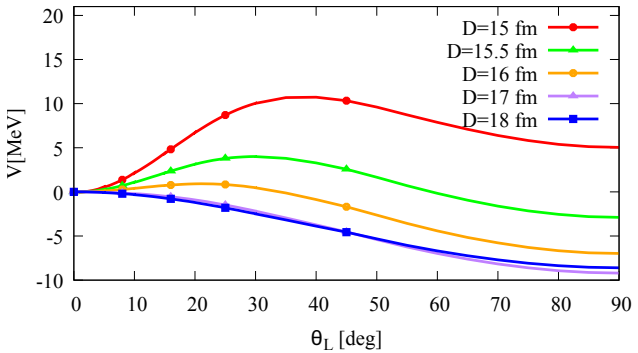

Two torques :

- attractive nucleus-nucleus torque
- repulsive Coulomb torque

Potential as a function of the light fragment angle

$^{144}Ba + ^{96}Sr$. D=15.5 and 20 fm

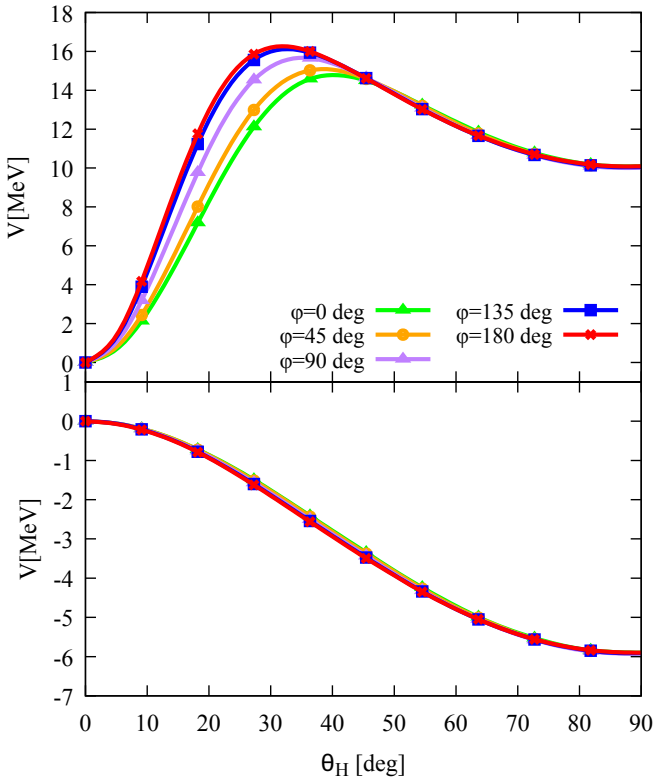

The azimuthal angle doesn't have an important role.

Frozen Hartree-Fock potential

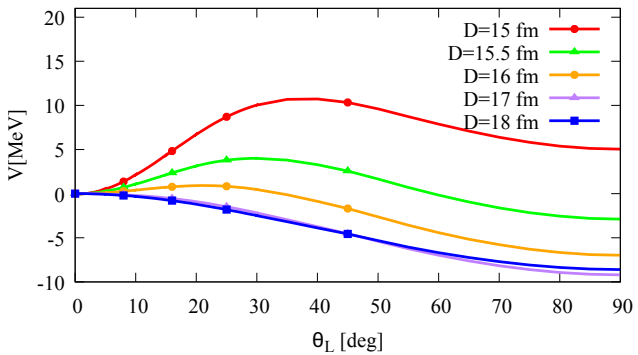

Two torques :

- attractive nucleus-nucleus torque
- repulsive Coulomb torque

4 degrees of freedom

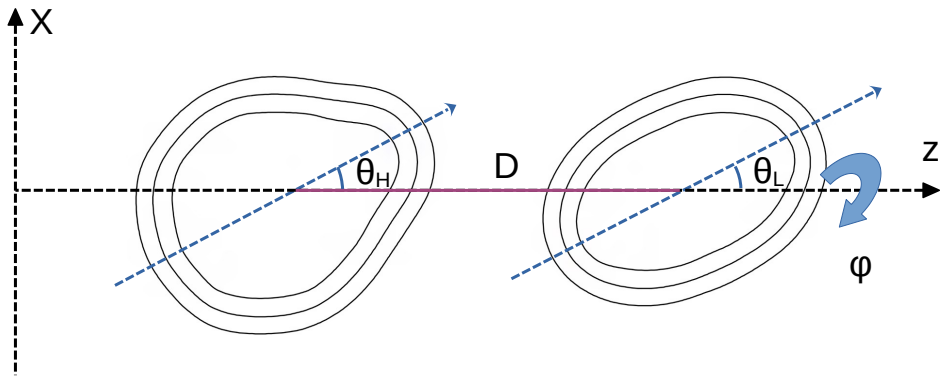

Hamiltonian

$$\hat{H}(D) = \frac{\hbar^2}{2I_H}\hat{L}_H^2 + \frac{\hbar^2}{2I_L}\hat{L}_L^2 + \frac{\hbar^2}{2I_\Lambda(D)}\hat{\Lambda}^2 + \hat{V}(\hat{\Theta}_H, \hat{\Theta}_L, \hat{\varphi}, D)$$

Solved in basis $|L_H, m, L_L, -m\rangle$

G. Scamps, G. Bertsch, Phys. Rev. C 108, 034616(2023).
Similar to the orientation pumping mechanism model Mikhailov, I. N., and Quentin, P. Physics Letters B, 462(1-2), 7-13 (1999)

Evolution of a one-angle wave packet assuming spherical ^{132}Sn

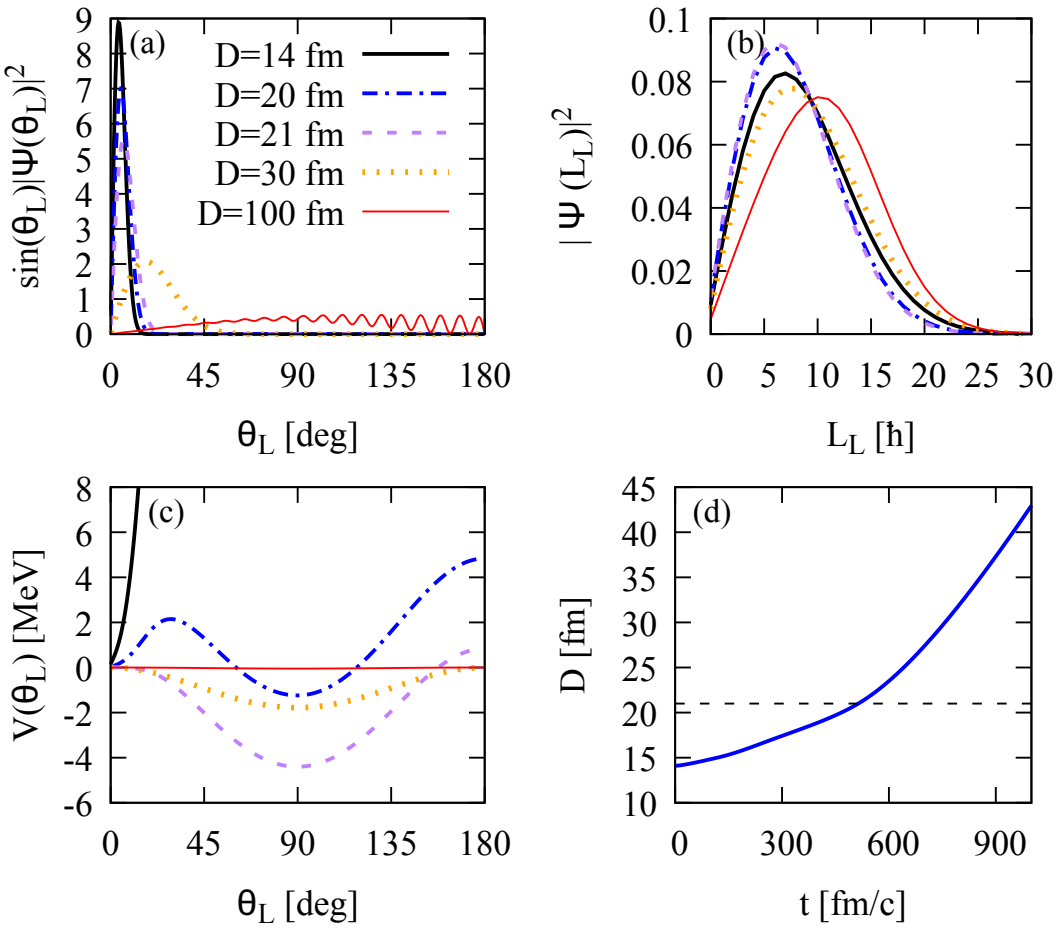

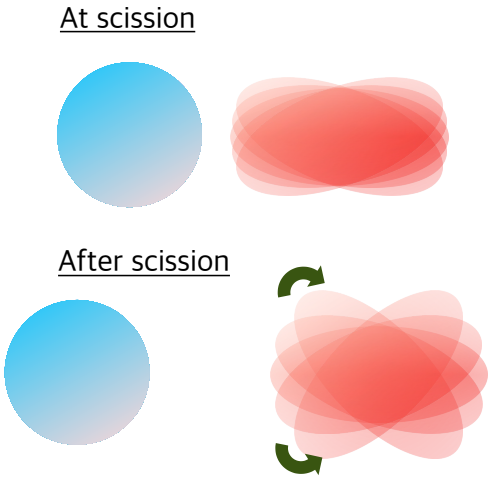

G. Scamps, G. Bertsch, Phys. Rev. C 108, 034616 (2023).

Effect of quadrupole deformation >> effect of $Z_1 Z_2$

TABLE II. Average spin$\langle L^2 \rangle^{\frac{1}{2}}$ in unit of $\hbar$ for the three fission fragments at scission ($D = 21$ fm) and at large distances. The last two columns show the same quantity with an MOI divided by 2.

Nucleus	Scission	Final	Scission ($I_{\frac{1}{2}}$)	Final ($I_{\frac{1}{2}}$)
^{108}Ru	9.28	12.31	7.24	10.38
^{144}Ba	10.04	10.95	7.70	8.66
^{96}Sr	7.74	9.30	6.03	7.62

also J. Randrup, PRC 108, 064606 (2023) : increase of 1 to 3 $\hbar$ due to the Coulomb torque.

New experimental data, neutronless $^{252}Cf \rightarrow {}^{120}Cd + {}^{132}Sn$

Cold fission selection TXE<8MeV

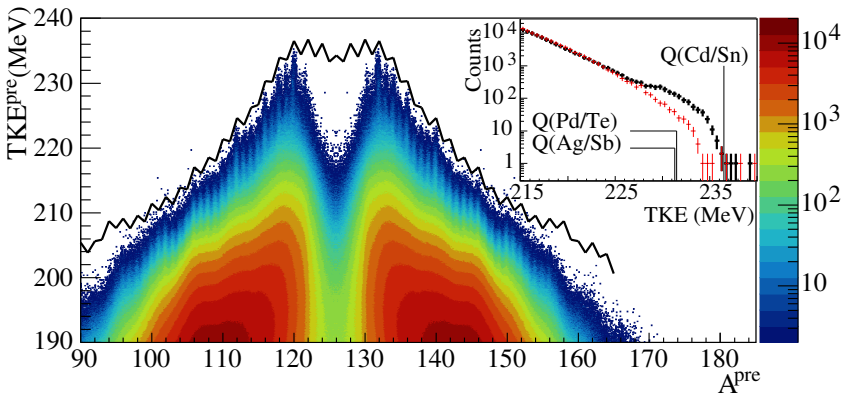

Results

- ^{132}Sn is found in ground-state
- The collective Hamiltonian model with β_2=0.42 reproduces the experimental γ-spectrum

γ-spectrum

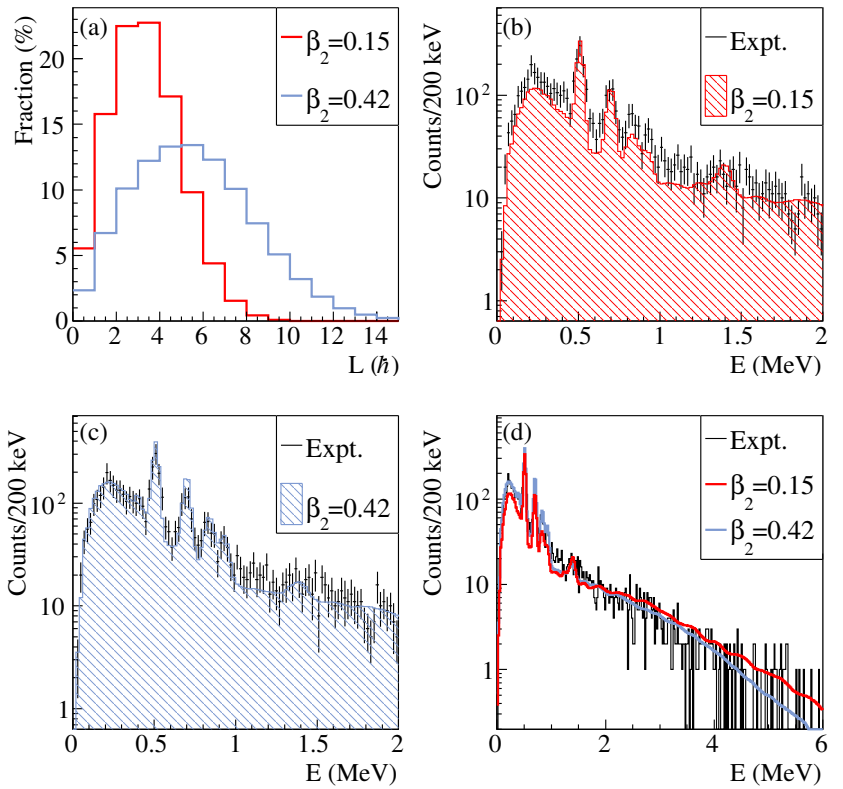

A. Francheteau, L. Gaudefroy, G. Scamps, O. Roig, V. Méot, A. Ebran, and G. Bélier, PRL 132, 142501 (2024).

Origin of angular momentum

The angular momentum of the compound nucleus originates from the **impact parameter** of the neutron.

Sharing during fission

During the fission dynamics, total angular momentum is conserved and shared between :

$$J_0 = \Lambda + J_L + J_H$$

- Λ : relative orbital motion of fragments
- J_L, J_H : intrinsic spins of the light and heavy fragments

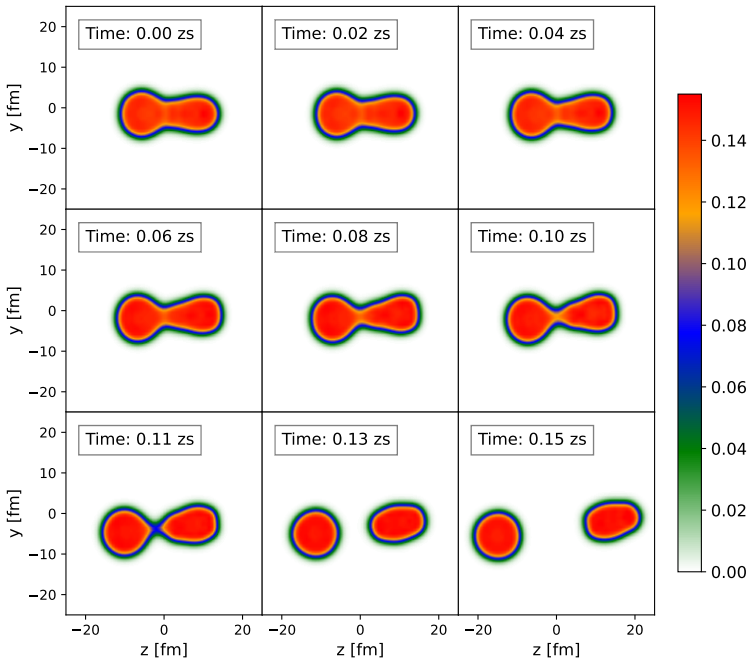

TDBCS dynamical evolution toward scission
$J_{tot} = 10\ \hbar$

Equilibrium interpretation

Assuming the fissioning system rotates uniformly before scission (R. Bass, *Nuclear Reactions with Heavy Ions*, Springer-Verlag, Germany, 1980) :

$$\frac{J_h}{I_h} = \frac{J_l}{I_l} = \frac{\Lambda}{I_\Lambda}$$

- I_h, I_l, I_Λ : moments of inertia of heavy, light fragments, and total system

Proportionality rule for fragment spins

$$J_i = \frac{I_i}{I_L + I_h + I_\Lambda} J_0, \quad i \in \{l, h\}$$

- Reproduces fragment spins at scission
- Light fragment spin continues to grow after scission due to Coulomb torque

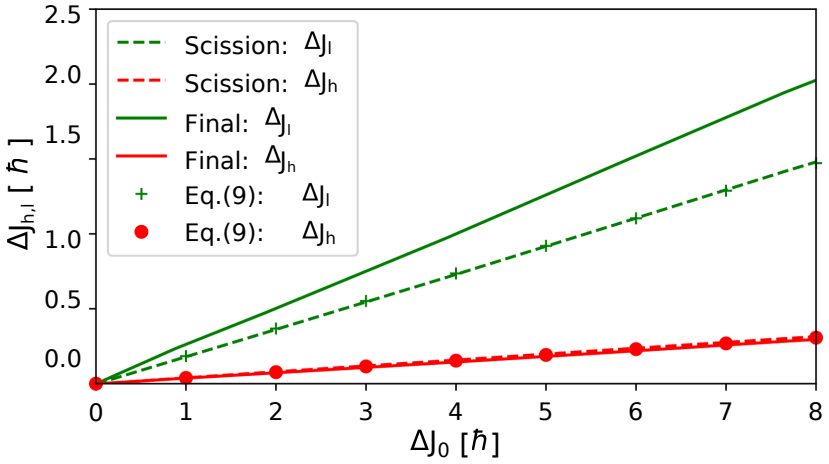

Figure – Fragment spins at scission (dashed) and at long distance (solid) vs total spin. TDHF+BCS simulations (lines) and equilibrium model (dots).

B. Fraïsse, G. Bélier, G. Scamps, L. Gaudefroy, V. Méot, et al. submitted

Role of TDDFT in fission dynamics

- Provides a fully microscopic description of nuclear reactions and fission dynamics
- Gives access to the **real-time evolution** of the many-body system
- Valuable to understand **mechanisms** :
  - generation of fragment spins
  - angular momentum sharing
  - coupling between shape and rotation

Connection to nuclear data ?

- For the moment, TDDFT is probably **not the best tool** for nuclear data
- Its main strength is to provide **physical insight** into reaction mechanisms
- Nevertheless, efforts are ongoing to extract **observable quantities** :
  - average fragment charge and masses
  - fragment spins
  - transfer of spin

Thank you for your attention

TDHFB framework

- Gogny-TDHFB code
- Gogny D1S interaction
- Hybrid basis :
  - 2D harmonic oscillator (x, y)
  - 1D spatial mesh (z)

Numerical setup

- $\Delta z = 0.8$ fm, $N_z = 52$
- $n_x + n_y \leq N_{\text{shell}} = 9$
- $\hbar\omega = 8$ MeV
- $\Delta t = 2 \times 10^{-3}$ zs

Physics case

- ^{230}Th
- ^{240}Pu
- ^{250}Cf

Asymmetric fission region
Heavy fragment influenced by octupole deformation
Connected to experimental saw-tooth spin pattern